



## RESEARCH ARTICLE

10.1002/2015JE004932

## Special Section:

The Mars Science Laboratory Rover Mission (Curiosity) at The Kimberley, Gale Crater, Mars

## Key Points:

- First mineralogical analysis of sandstone on Mars
- Windjana sandstone very rich in sanidine, implying a trachyte source rock
- The source of Gale Crater sediments is an incredibly diverse igneous terrane

## Supporting Information:

- Captions for Texts S1 and S2
- Texts S1 and S2
- Data Set S1
- Data Set S2

## Correspondence to:

A. H. Treiman,  
treiman@pi.usra.edu

## Citation:

Treiman, A. H., et al. (2016), Mineralogy, provenance, and diagenesis of a potassic basaltic sandstone on Mars: CheMin X-ray diffraction of the Windjana sample (Kimberley area, Gale Crater), *J. Geophys. Res. Planets*, 121, 75–106, doi:10.1002/2015JE004932.

Received 31 AUG 2015

Accepted 21 DEC 2015

Accepted article online 27 DEC 2015

Published online 29 JAN 2016

## Mineralogy, provenance, and diagenesis of a potassic basaltic sandstone on Mars: CheMin X-ray diffraction of the Windjana sample (Kimberley area, Gale Crater)

Allan H. Treiman<sup>1</sup>, David L. Bish<sup>2</sup>, David T. Vaniman<sup>3</sup>, Steve J. Chipera<sup>4</sup>, David F. Blake<sup>5</sup>, Doug W. Ming<sup>6</sup>, Richard V. Morris<sup>6</sup>, Thomas F. Bristow<sup>5</sup>, Shaunna M. Morrison<sup>7</sup>, Michael B. Baker<sup>8</sup>, Elizabeth B. Rampe<sup>6</sup>, Robert T. Downs<sup>7</sup>, Justin Filiberto<sup>9</sup>, Allen F. Glazner<sup>10</sup>, Ralf Gellert<sup>11</sup>, Lucy M. Thompson<sup>12</sup>, Mariek E. Schmidt<sup>13</sup>, Laetitia Le Deit<sup>14</sup>, Roger C. Wiens<sup>15</sup>, Amy C. McAdam<sup>16</sup>, Cherie N. Achilles<sup>2</sup>, Kenneth S. Edgett<sup>17</sup>, Jack D. Farmer<sup>18</sup>, Kim V. Fendrich<sup>7</sup>, John P. Grotzinger<sup>8</sup>, Sanjeev Gupta<sup>19</sup>, John Michael Morookian<sup>20</sup>, Megan E. Newcombe<sup>8</sup>, Melissa S. Rice<sup>21</sup>, John G. Spray<sup>12</sup>, Edward M. Stolper<sup>8</sup>, Dawn Y. Sumner<sup>22</sup>, Ashwin R. Vasavada<sup>20</sup>, and Albert S. Yen<sup>20</sup>

<sup>1</sup>Lunar and Planetary Institute, Houston, Texas, USA, <sup>2</sup>Department of Geological Sciences, Indiana University, Bloomington, Indiana, USA, <sup>3</sup>Planetary Science Institute, Tucson, Arizona, USA, <sup>4</sup>Chesapeake Energy Corporation, Oklahoma City, Oklahoma, USA, <sup>5</sup>NASA Ames Research Center, Moffett Field, California, USA, <sup>6</sup>Astromaterials Research and Exploration Science Division, NASA Johnson Space Center, Houston, Texas, USA, <sup>7</sup>Department of Geosciences, University of Arizona, Tucson, Arizona, USA, <sup>8</sup>Division of Geologic and Planetary Sciences, California Institute of Technology, Pasadena, California, USA, <sup>9</sup>Department of Geology, Southern Illinois University, Carbondale, Illinois, USA, <sup>10</sup>Department of Geological Sciences, University of North Carolina, Chapel Hill, North Carolina, USA, <sup>11</sup>Department of Physics, University of Guelph, Guelph, Ontario, Canada, <sup>12</sup>Department of Earth Sciences, University of New Brunswick, Fredericton, New Brunswick, Canada, <sup>13</sup>Department of Earth Sciences, Brock University, St. Catharines, Ontario, Canada, <sup>14</sup>Laboratoire Planétologie et Géodynamique de Nantes, LPGN/CNRS UMR6112, and Université de Nantes, Nantes, France, <sup>15</sup>Space Remote Sensing, Los Alamos National Laboratory, Los Alamos, New Mexico, USA, <sup>16</sup>NASA Goddard Space Flight Center, Greenbelt, Maryland, USA, <sup>17</sup>Malin Space Science Systems, Inc., San Diego, California, USA, <sup>18</sup>School of Earth and Space Exploration, Arizona State University, Tempe, Arizona, USA, <sup>19</sup>Department of Earth Science and Engineering, Imperial College, London, UK, <sup>20</sup>Jet Propulsion Laboratory, California Institute of Technology, Pasadena, California, USA, <sup>21</sup>Department of Earth Sciences, Western Washington University, Bellingham, Washington, USA, <sup>22</sup>Department of Earth and Planetary Sciences, University of California, Davis, California, USA

**Abstract** The Windjana drill sample, a sandstone of the Dillinger member (Kimberley formation, Gale Crater, Mars), was analyzed by CheMin X-ray diffraction (XRD) in the MSL Curiosity rover. From Rietveld refinements of its XRD pattern, Windjana contains the following: sanidine (21% weight, ~Or<sub>95</sub>); augite (20%); magnetite (12%); pigeonite; olivine; plagioclase; amorphous and smectitic material (~25%); and percent levels of others including ilmenite, fluorapatite, and bassanite. From mass balance on the Alpha Proton X-ray Spectrometer (APXS) chemical analysis, the amorphous material is Fe rich with nearly no other cations—like ferrihydrite. The Windjana sample shows little alteration and was likely cemented by its magnetite and ferrihydrite. From ChemCam Laser-Induced Breakdown Spectrometer (LIBS) chemical analyses, Windjana is representative of the Dillinger and Mount Remarkable members of the Kimberley formation. LIBS data suggest that the Kimberley sediments include at least three chemical components. The most K-rich targets have 5.6% K<sub>2</sub>O, ~1.8 times that of Windjana, implying a sediment component with >40% sanidine, e.g., a trachyte. A second component is rich in mafic minerals, with little feldspar (like a shergottite). A third component is richer in plagioclase and in Na<sub>2</sub>O, and is likely to be basaltic. The K-rich sediment component is consistent with APXS and ChemCam observations of K-rich rocks elsewhere in Gale Crater. The source of this sediment component was likely volcanic. The presence of sediment from many igneous sources, in concert with Curiosity's identifications of other igneous materials (e.g., mugearite), implies that the northern rim of Gale Crater exposes a diverse igneous complex, at least as diverse as that found in similar-age terranes on Earth.

### 1. Introduction

The Mars Science Laboratory spacecraft mission, through its rover Curiosity, has been exploring and investigating in Gale Crater, Mars, since its successful landing in August 2012. Curiosity's suite of sampling and analysis instruments was designed to investigate solid materials, their constituents (i.e., minerals), and the physical environment to characterize Mars' past environments in terms of potential habitability for life [Grotzinger et al., 2012, 2014, 2015a, 2015b]. Among Curiosity's instruments is the CheMin X-ray diffractometer [Blake et al., 2012],

©2015. The Authors.

This is an open access article under the terms of the Creative Commons Attribution-NonCommercial-NoDerivs License, which permits use and distribution in any medium, provided the original work is properly cited, the use is non-commercial and no modifications or adaptations are made.

which has determined the mineral contents, proportions, and compositions of several materials in Gale Crater [Bish *et al.*, 2013; Vaniman *et al.*, 2014]. CheMin results have shown that the windblown soil in Gale Crater has the mineralogy of a basalt, with no detectable crystalline water-bearing minerals [Bish *et al.*, 2013] and that the mudstones of the Yellowknife Bay area (Figure 1a) contain ferromagnesian smectite clays that formed in situ by aqueous alteration of olivine [Bristow *et al.*, 2015; Vaniman *et al.*, 2014].

After leaving the Yellowknife Bay area, Curiosity has traveled across the floor of Gale Crater (i.e., Aeolis Palus) toward its ultimate mission goal of investigating the stratigraphy of the central sedimentary mound in the Crater [Grotzinger *et al.*, 2012]. On this trek, Curiosity traversed across sedimentary rocks of the Bradbury group (Figure 2a) and investigated these rocks (by imaging, ChemCam Laser-Induced Breakdown Spectrometer (LIBS), and Alpha Proton X-ray Spectrometer (APXS)), at the Darwin and Cooperstown outcrops [Grotzinger *et al.*, 2015b; McLennan *et al.*, 2014]. These localities were not investigated in detail, because the MSL science team agreed to defer investigations until Curiosity reached the more extensive outcrops of these units in the Kimberley area [Grotzinger *et al.*, 2015b] (Figures 1 and 3).

Along its path, Curiosity encountered a wide range of clastic sedimentary rocks and clasts within or from those sediments [Sautter *et al.*, 2014; Schmidt *et al.*, 2014b; L. Le Deit *et al.*, The potassic sedimentary rocks in Gale crater, Mars as seen by ChemCam onboard Curiosity, submitted to *Journal of Geophysical Research Planets*, 2015] but did not stop to drill and obtain CheMin analyses of the mineralogies of these materials. Of particular interest along Curiosity's traverse have been the abundance and variety of sediments and rocks rich in the alkali elements (Na and K) and particularly those rich in potassium [Sautter *et al.*, 2014; Stolper *et al.*, 2013; Thompson *et al.*, 2014; L. Le Deit *et al.*, submitted manuscript, 2015]. The mineralogy of these sediments and rocks had been a matter of speculation. It was fortuitous that rocks in the Kimberley area, already targeted for detailed investigation, turned out to be among the most potassium rich analyzed in Gale Crater.

So on sol 609 ('sol' = Martian solar day since landing) of Curiosity's mission, a sandstone of the Kimberley area was drilled and delivered to CheMin for X-ray diffraction analysis of its mineralogy. Here we present the results of those analyses, in terms of mineralogy (mineral identities and cell parameters), elemental chemistry (in relation to APXS and ChemCam elemental analyses of rocks in the area), and regional geology for the Windjana area and the sources of its sediments from the far northern wall of Gale Crater.

### 1.1. Geological Setting for Kimberley and Windjana

Gale Crater is located on fluvially dissected highland crust, along Mars' highlands-lowlands "dichotomy" boundary [Anderson and Bell, 2010]. Crater counts on Gale's ejecta blanket and the underlying highland crust indicate that the Crater formed at ~3.7–3.6 Ga [Le Deit *et al.*, 2013; Thomson *et al.*, 2011]. The interior plains of Gale Crater (Aeolis Palus), Figure 1, contain fluvial valleys, eroded alluvial fan deposits, and sedimentary deposits that form a central mound (Aeolis Mons, informally Mount Sharp) cored by a possible central peak exposed on the south side of the mound [Le Deit *et al.*, 2013; Palucis *et al.*, 2014; Schwenzer *et al.*, 2012; Thomson *et al.*, 2011]. Sedimentary rocks in Gale Crater have been dated to  $4.21 \pm 0.35$  Ga, on Mars, by K-Ar systematics using data from the APXS and Sample Analysis at Mars (SAM) instruments on Curiosity [Farley *et al.*, 2014].

Prior to landing, the bedrock and surficial materials of Aeolis Palus in the vicinity of Curiosity's landing ellipse were mapped and subdivided into several units based on geomorphic, textural, and physical properties observed from orbit [Grotzinger *et al.*, 2014]. Following landing and the first two years of rover operations, these geomorphic/textural units were recognized to coincide with a succession of sedimentary rocks, approximately 75 m thick, that was designated the Bradbury group, Figure 2a [Grotzinger *et al.*, 2015b]. These rocks are interpreted to pass laterally into the Murray formation, a lacustrine mudstone that forms the basal unit of Mount Sharp [Grotzinger *et al.*, 2015b].

The Bradbury group is composed largely of fluvial clastic sediments (conglomerates through mudstones), with interstratified eolian sandstones and siltstones (Figures 2a and 2b) [Grotzinger *et al.*, 2015b]. Fluvial deposits were derived from the Gale Crater northern wall and rim based on southerly directed paleocurrent direction [Grotzinger *et al.*, 2015b]. Eolian deposits show variable transport directions that suggest reworking of underlying fluvial sands. The Bradbury group is largely undivided with the exception of the basal Yellowknife Bay formation and the Kimberley formation in the middle of the group.

Between sols 574 and 631, the well-exposed outcrops in the Kimberley area (Figures 1a and 1b) were studied in detail; the rocks are all assigned to the Kimberley formation. The stratigraphic setting of the Kimberley

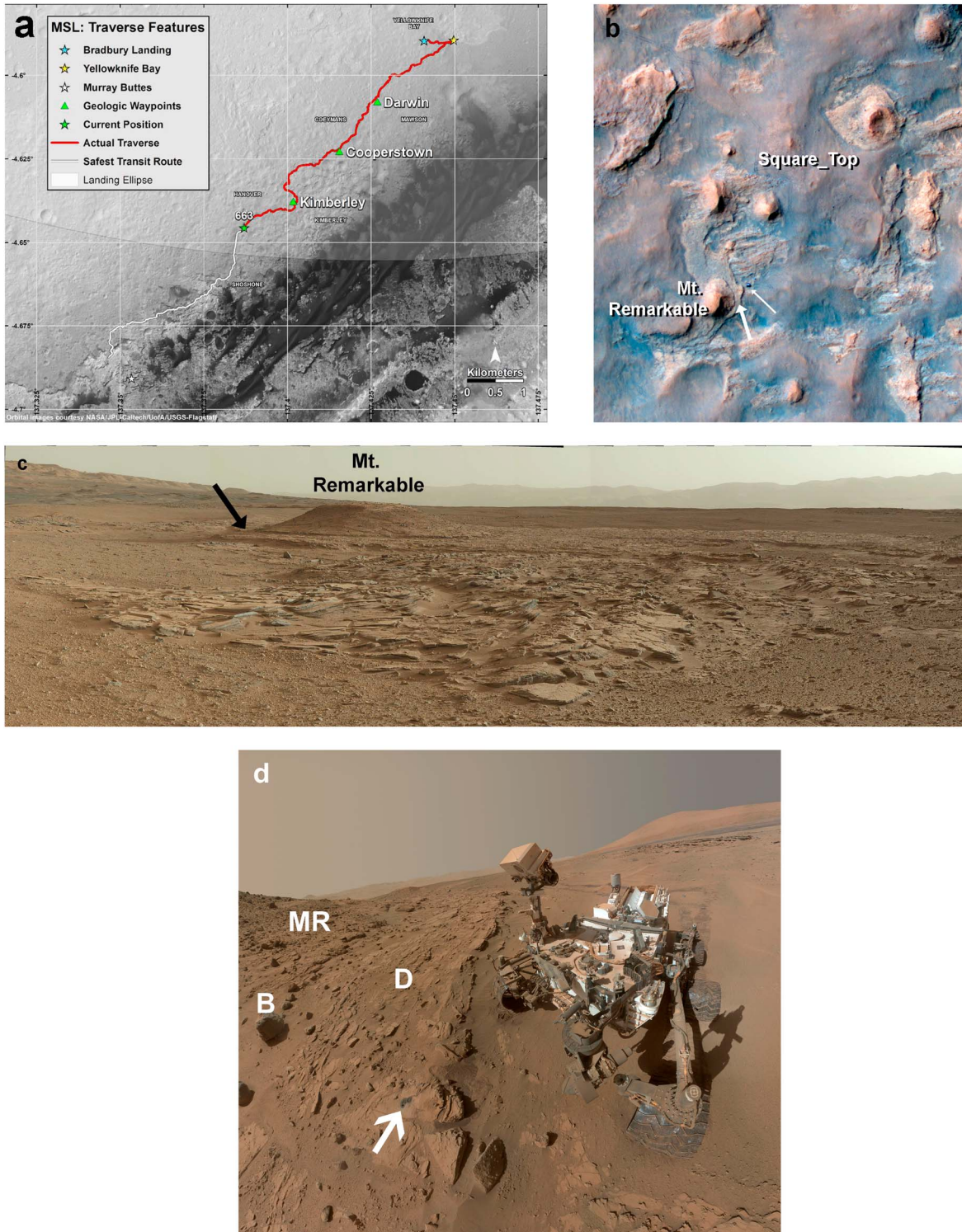


**Figure 1.** Regional geology and local setting of the Kimberley area and Windjana site. Images from NASA, JPL, Malin Space Science Systems, and the University of Arizona. (a) Curiosity's traverse across Gale Crater, with the Kimberley site (NASA image PIA 18392). (b) HiRISE image of Kimberley area with rover and Windjana site noted. Heavy arrow indicates Windjana drill site; light arrow denotes Curiosity rover. (NASA image PIA 18018). (c) View of Kimberley area from near the Square\_Top location (see Figure 1b). Undulating beds of Square\_Top member in foreground; Windjana drill site noted by arrow; Rim of Gale crater in distance to right and center. From Curiosity MastCam mosaic mcam02484, acquired on sol 590. (d) MAHLI self-portrait of Curiosity in front of the Windjana site. Arrow shows Windjana drill site, with main and mini-drill holes. Dillinger (D) and Mount\_Remarkable (MR) units labeled, as is a fragment of rock from the Beagle (B) unit that rolled down the hill. Note the central mound in Gale crater (Mount Sharp) in top right of image. From NASA image PIA 18930.

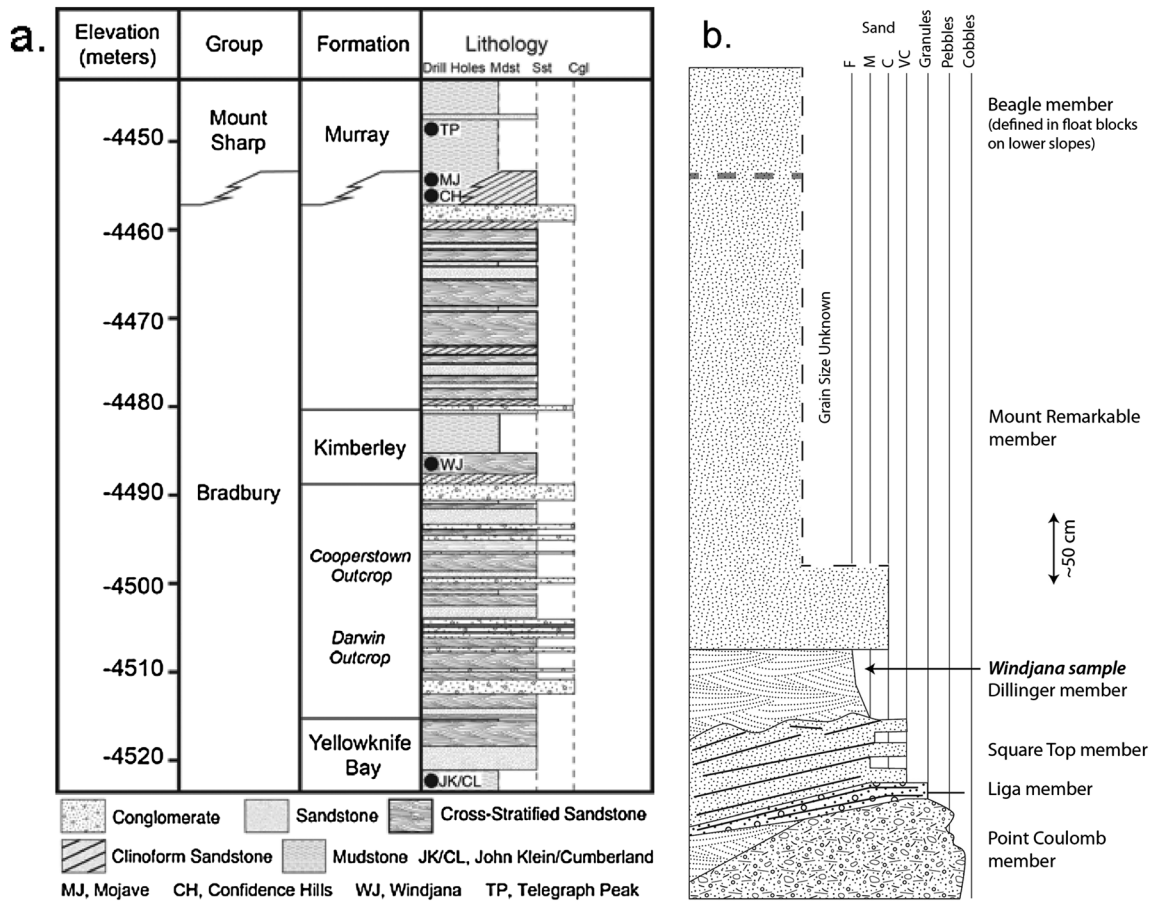


**Figure 2.** Stratigraphic sections for Curiosity's traverse in Gale Crater of the Kimberley formation (after D. Sumner). (a) Stratigraphic section of the Bradbury Group sediments. Detailed information was obtained only for the Yellowknife Bay and Kimberley formations, and for isolated outcrops of the intervening section [Grotzinger *et al.*, 2015a, 2015b]. The Murray Formation, the lowest portion of the Mount Sharp sediments, is interpreted to overlie and interfinger with the uppermost Bradbury Group. Black dots with two-letter designators are stratigraphic locations of samples analyzed by CheMin. (b) Detailed section of the Kimberley formation. The lowest exposed member, Point\_Coulomb, is conglomeratic and is overlain by flat-lying laminar sandstone of the Liga member. Next up are the undulating cross-bedded sandstones of the Square\_Top member and then the cross-bedded (but more massive) Dillinger member. The Windjana sample is of the Dillinger member. It is overlain by the massive, poorly bedded sandstone of the Mount\_Remarkable member; above that is the massive dark rock of the Beagle member, analyzed only as float and not shown on the column. Vertical scale bar (arrows) is 50 cm; horizontal scale indicates grain size in the sediments, showing the fining upward nature of the section. Sediment sizes are: Cobble (64 mm–256 mm); Pebble (4 mm–64 mm); Granule (2 mm–4 mm); Sand VC, very coarse (1 mm–2 mm); Sand C, coarse (500 μm to 1 mm); Sand M, medium (250–500 μm); and Sand F, fine (125–250 μm).

formation is described by Grotzinger *et al.* [2015a], Grotzinger *et al.* [2015b], and Stack *et al.* [2015], and its chemostratigraphy is described by Le Deit *et al.* [2015], and L. Le Deit *et al.* (submitted manuscript, 2015). Facies similar to those of the Kimberley formation have been observed in the same stratigraphic sequence at several locations near the Kimberley area; Curiosity studied these rock types previously along its traverse through Moonlight Valley and Violet Valley (sols 500–552), and again at the Kylie location (sols 552–559) [Edgar *et al.*, 2014; Grotzinger *et al.*, 2015a].

The Kimberley formation includes several distinct subdivisions, here designated as members, each of which is a few tens of centimeters to a few meters thick (Figures 2a and 2b). The basal Point Coulomb and Liga members are interpreted as fluvial conglomerates. Overlying the Liga is the Square Top member, which is interpreted as deltaic sandstones and pebbly sandstones. In turn, the Dillinger member of uncertain depositional origin, overlies the Square Top member. The poorly exposed Mount Remarkable member tops the succession along with remnants of a capping sandstone unit, the Beagle member. Outcrops of the Liga and Dillinger members are marked by linear ridges of material that is relatively resistant to erosion. Several such ridges are near the Windjana drill location (Figure 3a), and the one investigated in detail (named Stephen) is strongly enriched in manganese [Lanza *et al.*, 2014].

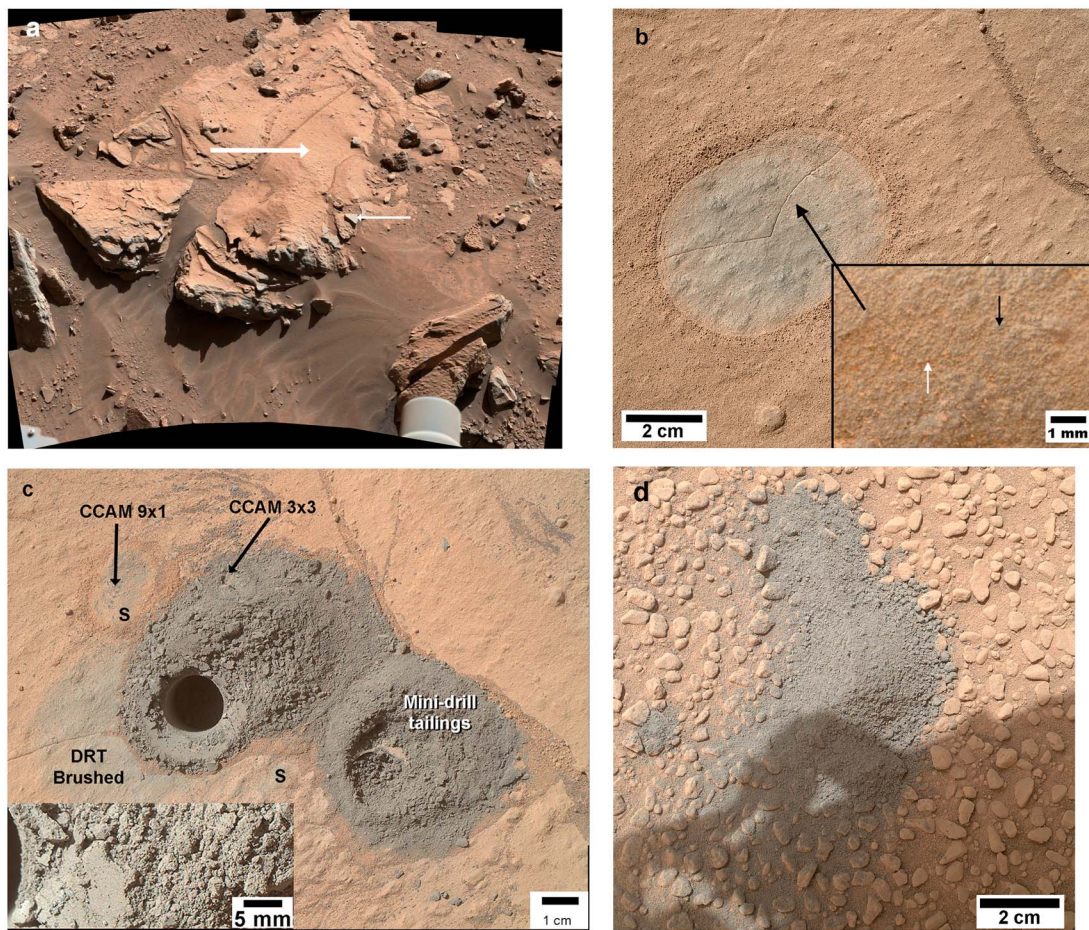


**Figure 3.** Local views of the Windjana outcrop and sample. Images care of NASA, JPL, and Malin Space Science Systems. (a) MastCam mosaic of the Windjana drill target and surroundings (NASA image PIA 18087). Large arrow indicates the drill site for the Windjana sample; small arrow shows Mn-rich platy veinlets or alterations (target Stephen, [Lanza *et al.*, 2014]). (b) The Windjana drill target, after brushing with the MSL DRT tool (NASA image PIA 18088; MAHLI image 0612MH0003880010203325C00). The brushed area is darker than the rusty colored dust. Inset to bottom right shows detail (location at heavy black arrow). White arrow denotes a clump of dust produced during brushing,  $\sim 100\ \mu\text{m}$  across. Black arrow denotes a pair of dark sediment grains, each  $\sim 80\ \mu\text{m}$  across, with sand grains averaging  $\sim 100\ \mu\text{m}$  across. From MAHLI image 0612MH0003860010203339C00. (c) Windjana sample area after drilling and analyses. “CCAM 1x9” and CCAM 3x3” are locations of ChemCam rasters of Windjana bulk and Windjana drill fines respectively. “S” are marks from drill stabilizers. Inset shows detail of drill cuttings, with no distinct grains  $> 100\ \mu\text{m}$  (3 pixels). Mosaic of MAHLI images 0627MH0001900010203476C00, 0627MH0001900010203478C00, 0627MH0001900010203510C00 *c/o* MAHLI team; inset from image 0627MH0001900010203480C00. (d) Dump of the Windjana sample from the SaH/SPaH, sol 704, onto a dusty surface composed of rounded pebbles. Shadow from rover arm at bottom of image. The APXS analysis of Table 2 is of this material (from MAHLI image 0704MH0001900010204151C00).

The Dillinger member of the Kimberley formation was sampled for CheMin and SAM analyses during drilling of a target named “Windjana.” There, the Dillinger is composed of fine-grained sandstone to siltstone. The Dillinger member is marked by low-angle cross stratifications that dip generally northward, whereas the regional paleo-depositional dip of fluvial facies of the Kimberley formation is toward the south; this difference may suggest that the Dillinger member is eolian (J. Grotzinger, personal communication, 2015). The Dillinger and the subjacent Square Top and Liga members (fluvial sandstones) all have anomalously high  $\text{K}_2\text{O}$  abundances compared to most other rocks encountered in Gale Crater [Grotzinger *et al.*, 2014; L. Le Deit *et al.*, submitted manuscript, 2015].

## 2. Samples and Methods

### 2.1. Sample and Acquisition

On sol 580 of the mission, Curiosity arrived at the northernmost outcrops of Kimberley area and investigated the rocks of the Square Top and Liga members (Figure 1). Curiosity approached the Windjana drill site on sol 608, tested it with a minidrill on sol 615 for rock properties and stability, and acquired a drilled sample on sol

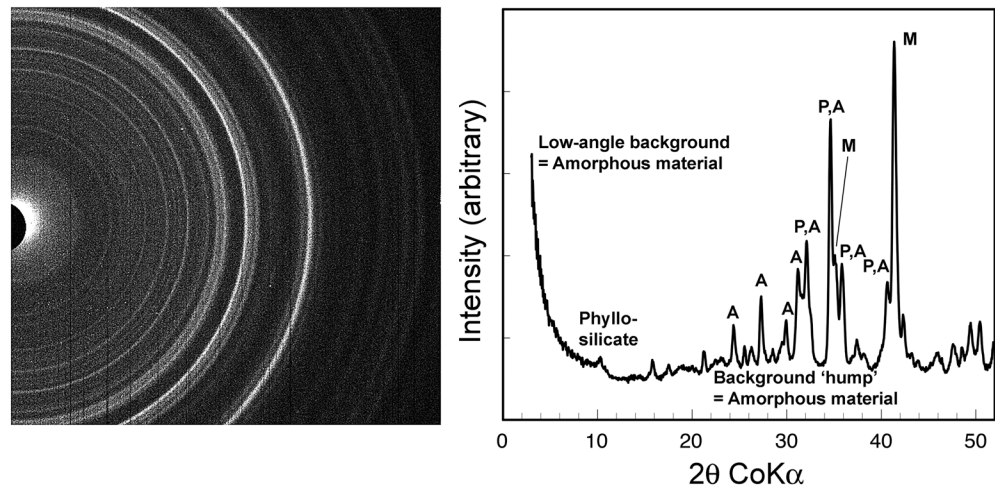


**Figure 4.** CheMin X-ray diffraction results for the Windjana sample. (a) Diffraction image from CheMin. Sum of all data for the Windjana sample in the unused CheMin cell; beam is black semicircle to left; light-toned rings are diffractions; dark vertical stripes are flaws in the CCD X-ray detector. (b) One-dimensional diffraction pattern, radially integrated from the diffraction image. Annotations are as follows: A, alkali feldspar; P, pyroxenes; M, magnetite.

621 (Figure 3) [Anderson *et al.*, 2012, 2015a]. The drilled sample was sieved on sol 622 to  $<150\ \mu\text{m}$  in the CHIMRA sample processing system and delivered then to CheMin into an unused Mylar cell (# 13A) for CheMin diffraction analysis and also to SAM for evolved gas analyses. The Curiosity rover departed from Windjana and the Kimberley area on sol 630 en route to its next detailed investigations at Pahrump Hills (Figure 1a) and to Mount Sharp, the central mound of Gale Crater. During this traverse, a second aliquot of Windjana sieved material was delivered on sol 640 to a Mylar cell (#12B) that had been used previously and dumped.

## 2.2. Methods and Data

All data used here have been released to the public and are available through the Planetary Data System (<https://pds.nasa.gov>) and other sources.

### 2.2.1. CheMin

Diffraction patterns for the Windjana powder, as two-dimensional images from the CheMin CCD [Blake *et al.*, 2012], were acquired for a total of 23 h over sols 623–632. There were no systematic differences among the individual images (i.e., in overall intensity or in relative strengths of diffraction peaks), so all were summed to yield a single two-dimensional diffraction pattern (Figure 4a). The second aliquot, delivered on sol 640 to a used and dumped Mylar cell (#12B), was analyzed for 22 h over sols 640–656. Results for Windjana material in this cell are qualitatively identical to those for the pristine cell but show evidence that some material remained in the cell from the previous analysis of Cumberland, a mudstone from an earlier location; these data are not considered further.

The two-dimensional CCD diffraction images were corrected on the spacecraft for DC offset and some hot pixels (pixels on the CCD which register high values in the absence of light or X-ray hits), summed and manually corrected for other hot pixels on the ground, and converted to a conventional one-dimensional X-ray diffraction pattern (Figure 4b) using the computer code “GSE\_ADA<sup>®</sup> for NASA”, beta version 1.09 [Dera *et al.*, 2013], see supporting information. The GSE\_ADA code sums diffraction events circumferentially around the two-dimensional diffraction image, given the following parameters: the distance from sample to CCD, the location of the X-ray beam center, the shape of the beam, and the tilt of the CCD surface with respect to the X-ray beam. The values of these parameters were obtained by analysis of beryl in an onboard CheMin standard, using its cell dimensions determined with laboratory X-ray diffractometers on Earth.

Procedures for processing and interpreting the Windjana X-ray diffraction pattern are as described earlier for CheMin [Bish *et al.*, 2013; Blake *et al.*, 2012, 2013; Vaniman *et al.*, 2014]. The Windjana diffraction data were first evaluated by comparisons and searches of the International Centre for Diffraction Data<sup>®</sup>

**Table 1.** Refined Unit Cell Parameters of Well-Crystalline Minerals in the Windjana Sandstone<sup>a</sup>

Mineral	<i>a</i> (Å)	<i>b</i> (Å)	<i>c</i> (Å)	<i>α</i> (deg)	<i>β</i> (deg)	<i>γ</i> (deg)
Sanidine	8.596(12)	13.047(11)	7.183(5)	-	115.97(7)	-
Plagioclase <sup>b</sup>	8.166(90)	12.87(10)	7.126(110)	93.5(20)	116.5(7)	90.0(9)
Olivine	4.790(7)	10.298(9)	6.031(7)	-	-	-
Augite	9.761(6)	8.94(1)	5.28(1)	-	106.3(2)	-
Pigeonite	9.67(1)	8.905(13)	5.215(5)	-	108.7(1)	-
<i>Enstatite</i>	<i>18.4(2)</i>	<i>8.9(1)</i>	<i>5.19(1)</i>	-	-	-
Magnetite	8.3856(11)	-	-	-	-	-
Ilmenite	5.081(7)	-	14.04(4)	-	-	-
Hematite	5.02(2)	-	13.87(14)	-	-	-
<i>Pyrrhotite</i>	<i>6.85(4)</i>	-	<i>16.99(8)</i>	-	-	-
<i>Akaganeite</i>	<i>10.61(3)</i>	<i>3.1(1)</i>	<i>10.5(3)</i>	-	<i>90.4(16)</i>	-
Apatite	9.428(16)	-	6.87(3)	-	-	-
<i>Anhydrite</i>	<i>6.98(3)</i>	<i>7.01(3)</i>	<i>6.20(2)</i>	-	-	-
<i>Bassanite</i>	<i>11.9(2)</i>	<i>6.97(4)</i>	<i>12.70(8)</i>	-	<i>86(7)</i>	-

<sup>a</sup>Numbers in parentheses are 1 $\sigma$  uncertainties on the cell parameters, applied to their last digits. Italics indicate that the mineral is near its detection limit, and so has uncertain unit cell parameters.

<sup>b</sup>For plagioclase, cell parameters are the averages from the three most similar refinements, and the uncertainties are 1 $\sigma$  for all refinements.

Powder Diffraction File using the software packages Jade<sup>®</sup> (Materials Data Incorporated, Livermore, California) and Topas<sup>®</sup> (Bruker AXS). CheMin's relatively low  $2\theta$  resolution ( $\sim 0.3^\circ$   $2\theta$  full width at half maximum at  $25^\circ$   $2\theta$ ) limits its capability to identify and determine abundances of minor crystalline phases ( $< 3$  wt %). The 1-D XRD patterns were analyzed with Rietveld methods, using Topas<sup>®</sup> and JADE<sup>®</sup>. In the Rietveld method, one constructs a model for the diffraction pattern from the crystal structures and compositions of its component phases, and the difference between the measured and model patterns is minimized by varying parameters in the model, including scale factors (related to phase abundance), unit cell parameters, crystallite size, and strain broadening. Atomic positions and site occupancies were not varied, except for proportions of octahedrally coordinated cations (Fe, Mg, Ca) in olivine and pyroxenes, and Na-Ca in plagioclase (Tables 1 and 2).

The CheMin team produced six independent Rietveld refinements using MDI Jade<sup>®</sup> and Bruker AXS Topas<sup>®</sup>, and the results here are the average or consensus of those refinements (Tables 1 and 2). Individual refinements can differ because of choices of input parameters (e.g., unit cell parameters and crystal structures for each given mineral), choices of constraints on the extent of variation permitted (e.g., limiting unit cell parameters to be within a given range), and choices of minerals to include in the model. In addition, several of the input minerals have similar diffraction patterns (e.g., pigeonite, enstatite, and augite), which can proxy for each other in refinement, particularly when they are present in small amounts. For example, the six independent refinements all yielded approximately the same proportions of total pyroxene, but they differed somewhat as to proportions of individual pyroxenes. Results of the individual refinements are given in the supporting information.

Proportions of amorphous and poorly crystalline phases in the Windjana sample (Table 2) were calculated from the diffraction pattern using computer code FULLPAT [Chipera and Bish, 2002]. FULLPAT creates models of the target diffraction pattern as sums of library patterns (including those on amorphous and poorly crystalline minerals) and minimizes the difference between the model and target patterns. The calculated proportions of amorphous and poorly crystalline phases are uncertain, in great part because their chemical compositions (and thus X-ray scattering strengths) are not known. We estimate, for Windjana, that the proportions are uncertain to 1 $\sigma$  of 20% of the amounts present.

### 2.2.2. Chemical Compositions

The chemical composition of the Windjana sample, on which much of this analysis relies, comes from the APXS instrument on the rover arm [Campbell et al., 2012; Thompson et al., 2014]. Additional detail is available in Gellert et al. [2014a, 2014b]. The APXS acquired several chemical compositions of the Windjana rock and drill powders (Table 3); of those, we rely on the analysis of the Windjana dump sample, which was the sieved powder remaining in the CHIMRA delivery system after aliquots had been delivered to SAM and CheMin. This is the best available analog for what was delivered to CheMin and SAM.

**Table 2.** Mass Proportions of Phases in the Windjana Sandstone and Other Gale Crater Samples<sup>a</sup>

Mineral	Windjana		John Klein Mass % Total	Cumberland Mass % Total	Rocknest Mass % Total
	Mass % Crystalline	Mass % Total			
Sanidine	28(4)	21(3)	1.2	1.6	0.9
<i>Oligoclase</i>	1.0(16)	0.8(1.2)	-	-	-
<i>Andesine</i>	2(2)	2(2)	-	-	-
Plagioclase total	3(3)	3(3)	22.4	22.2	29.8
Olivine	6.0(14)	4.7(10)	2.8	0.9	16.4
Augite	26(3)	20(3)	3.8	4.1	10.7
Pigeonite	15(3)	11(2)	5.6	8.0	10.1
Enstatite	<i>det?</i>	<i>det?</i>	3.0	4.1	-
Magnetite	16(3)	12(2)	3.8	4.4	1.5
Ilmenite	1.1(7)	0.8(5)	-	0.5	0.7
Hematite	0.7(5)	0.6(4)	0.6	0.7	0.8
Pyrrhotite	0.4(4)	0.3(3)	1.0	1.0	-
Akaganeite	0.3(3)	0.2(2)	1.1	1.7	-
Anhydrite	0.6(4)	0.4(3)	2.6	0.8	1.1
Bassanite	0.7(5)	0.5(4)	1.0	0.7	-
Jarosite	<i>det?</i>	<i>det?</i>			
Fluorapatite	1.1(10)	0.8(8)			
Quartz	-	-	0.4	0.1	-
Halite	-	-	0.1	0.1	-
Pyrite	-	-	0.3	-	-
<i>Kaolinite</i>	<i>det?</i>	<i>det?</i>	-	-	-
Smectite/illite	-	10(2)	22	18	-
Amorphous	-	15(3)	28	31	27

<sup>a</sup>Weight % in crystalline mass includes all well-crystalline materials and excludes phyllosilicates and amorphous material; based on Rietveld refinements. Mass % total includes phyllosilicates and amorphous material; based on Rietveld refinements and FULLPAT analysis. Numbers in parentheses are 1  $\sigma$  uncertainties on values; see Data Set S1 in the supporting information. Italics indicate that a phase is near its detection limit. "det?" indicates possible detection; present in a few of the Rietveld refinements.

It is possible that the sieved powder delivered to CheMin does not have the composition of the bulk rock because of grain separation and fractionation during drilling and sieving. A suggestion to this effect can be seen in Table 3 by comparing the drill fines (sol 662) with the sieve dump (sol 704); the latter is poorer in K<sub>2</sub>O, and richer in Na<sub>2</sub>O and SO<sub>3</sub> than the former. However, the drill fines are from a different range of depths within the rock than the sample ingested into CHIMRA, and that difference may account for the range in bulk compositions (Table 3). In either case, we assume that the sieved sample analyzed by CheMin is representative of the bulk Windjana rock.

Information on the volatile constituents in rocks of the Kimberley comes from the EGA (evolved gas) instrument in the SAM instrument suite [Mahaffy *et al.*, 2012]. SAM EGA analysis can provide constraints on the identity, abundance, and isotope ratios of volatile constituents, like carbonate and nitrate, that decompose or devolatilize below ~900°C. Data on the Windjana sample are from McAdam *et al.* [2015] and Stern *et al.* [2015b].

To understand the local context of the chemistry of the Windjana sample, we rely on data from the ChemCam LIBS instrument [Wiens *et al.*, 2012], which can probe the chemistry of rocks up to a few meters from the rover. We use the June 2015 recalibration of the LIBS results (available from the NASA Planetary Data System); comprehensive views of chemostratigraphy in the Kimberley area are given in a companion paper (L. Le Deit *et al.*, submitted manuscript, 2015). We do not compare chemical analyses by APXS and LIBS directly because of known offsets between these two methods.

### 2.2.3. Other Data

Images of the Windjana sample area and the Kimberley area are from the Mars Hand Lens Imager (MAHLI) and MastCam imagers on the Curiosity Rover. Spectral reflectance constraints on the iron-bearing minerals of the Windjana sample come from "passive spectra" in visible light from the ChemCam instrument [Johnson *et al.*, 2015a, 2015b; Wiens *et al.*, 2012].



**Table 3.** APXS Chemical Analyses of the Windjana Sandstone, and Calculated Compositions of Its Crystalline and Amorphous + Poorly Crystalline Materials

Sol (wt %)	612 Pre-DRT	612 Post-DRT	622 DrillFines <sup>a</sup>	704 DumpPile	$\pm 2\sigma$	Crystalline Component	$\pm 2\sigma^b$	Amorphous + Poorly Crystalline	$\pm 2\sigma^b$
SiO <sub>2</sub>	39.84	40.47	39.30	37.38	0.86	43.5	7.8	14.2	19.5
TiO <sub>2</sub>	1.02	1.03	1.15	1.07	0.06	0.6	0.7	2.6	2.6
Al <sub>2</sub> O <sub>3</sub>	6.83	5.62	5.69	5.62	0.38	5.8	2.0	4.7	5.6
Cr <sub>2</sub> O <sub>3</sub>	0.41	0.42	0.44	0.49	0.02	0.0	0.0	2.0	1
Fe <sub>2</sub> O <sub>3</sub>	-	-	-	-	-	12.1	4.9	-	-
FeO	23.38	24.51	26.50	27.90	0.66	14.2	3.8	33.8	21.6
MnO	0.65	0.67	0.56	0.53	0.02	0.28	0.08	1.3	0.5
MgO	9.18	10.87	12.67	12.29	0.50	9.1	2.3	21.6	9.6
CaO	5.50	5.01	4.91	5.26	0.12	6.5	2.1	0.9	7.3
Na <sub>2</sub> O	2.09	1.21	0.40	0.96	0.14	0.34	0.36	2.9	1.8
K <sub>2</sub> O	1.71	3.01	3.65	3.09	0.20	4.45	2.6	-1.6	4.8
P <sub>2</sub> O <sub>5</sub>	0.90	0.81	0.73	0.64	0.10	0.6	0.8	0.8	3.0
SO <sub>3</sub>	6.42	3.95	2.58	3.57	0.10	1.0	1.0	11.8	6.2
Cl	1.33	1.65	0.80	0.57	0.02	0.0	0.0	2.4	1.2
Total	99.26	99.23	99.4	99.37		98.3	15.2	97.3	5.8
Ni ppm	410	383	383	516	30				
Zn ppm	3584	3981	4347	4775	145				
Br ppm	1819	1979	348	123	5				

<sup>a</sup>DrillFines is Raster Point 3, which was the longest duration analysis with the lowest uncertainties.

<sup>b</sup>Based on Monte Carlo propagation of uncertainties in bulk composition, mineral compositions, and mineral abundances; averages and standard deviations of 2500 runs. See Data Sets S1 and S2 in the supporting information.

### 3. Results

#### 3.1. Rock Classification

The Windjana sample is clearly of a clastic sedimentary rock, because its source rock contains discrete grains (Figure 3b) and is within a stratigraphic sequence of other clastic rocks. The MAHLI images of the Windjana outcrop with the greatest spatial resolution show rare grains up to ~400  $\mu\text{m}$  across, and most of the detectable grains are ~80  $\mu\text{m}$  across (with a limit of detection of three pixels, i.e., 48  $\mu\text{m}$ ). These images suggest that the dominant grain size is < 125  $\mu\text{m}$ , which (in the standard classification of sedimentary rocks) would make the Windjana sample a very fine sandstone or a siltstone or a mudstone. For simplicity, we refer to the Windjana rock as a sandstone.

#### 3.2. Minerals and Compositions

##### 3.2.1. Alkali Feldspar

The most distinctive mineralogical feature of the Windjana sandstone is its abundance of alkali feldspar, 28% by mass of the crystalline material (Table 2) and 21% by mass of the whole rock (including amorphous and poorly crystalline components). This abundance of alkali feldspar is reflected also in the significant abundance of K<sub>2</sub>O in the bulk composition (Table 3); both will be crucial facts for understanding the sources and genesis of the Windjana sandstone.

Alkali feldspars have a range of compositions and crystal structures. Compositional variability is mostly from the substitution of Na<sup>+</sup> for K<sup>+</sup>, although other substitutions can be significant, including: B<sup>3+</sup> for Al<sup>3+</sup>, Fe<sup>3+</sup> for Al<sup>3+</sup>, NH<sub>4</sub><sup>+</sup> and/or Rb<sup>+</sup> for K<sup>+</sup>, and Ba<sup>2+</sup> + Al<sup>3+</sup> for K<sup>+</sup> + Si<sup>4+</sup> [Cerny and Chapman, 1986]. Structural variability comes from the ordering (or distribution) of the tetrahedral Al<sup>3+</sup> among the four (potentially) distinct tetrahedral sites in the structure [Kroll and Ribbe, 1983]. Depending on whether the Al<sup>3+</sup> is completely ordered, partially ordered, or completely disordered, the KAlSi<sub>3</sub>O<sub>8</sub> mineral would be identified as microcline, orthoclase, or sanidine, respectively (Figure 5). Although the name “sanidine” can connote an igneous origin, its use here is in its strict mineralogical sense, as K-rich feldspar with extensive Al-Si disorder.

Fortunately, the *b* and *c* crystal unit cell parameters of alkali feldspars vary in a monotonic and distinctive fashion with Na/K ratio and Al-Si ordering [Blasi, 1977; Kroll and Ribbe, 1983, 1987; Wright and Stewart, 1968], and the CheMin determinations for the Windjana alkali feldspar (Table 1) are sufficient for its classification. Figure 5 shows the *b* and *c* cell parameters of the Windjana alkali feldspar compared to those of other alkali feldspars, based on the extensive experiments and literature compilations of Kroll and Ribbe [1983]. The Windjana alkali feldspar plots are within uncertainty of being pure KAlSi<sub>3</sub>O<sub>8</sub>, although the *b*-*c* plot is not sensitive to Na

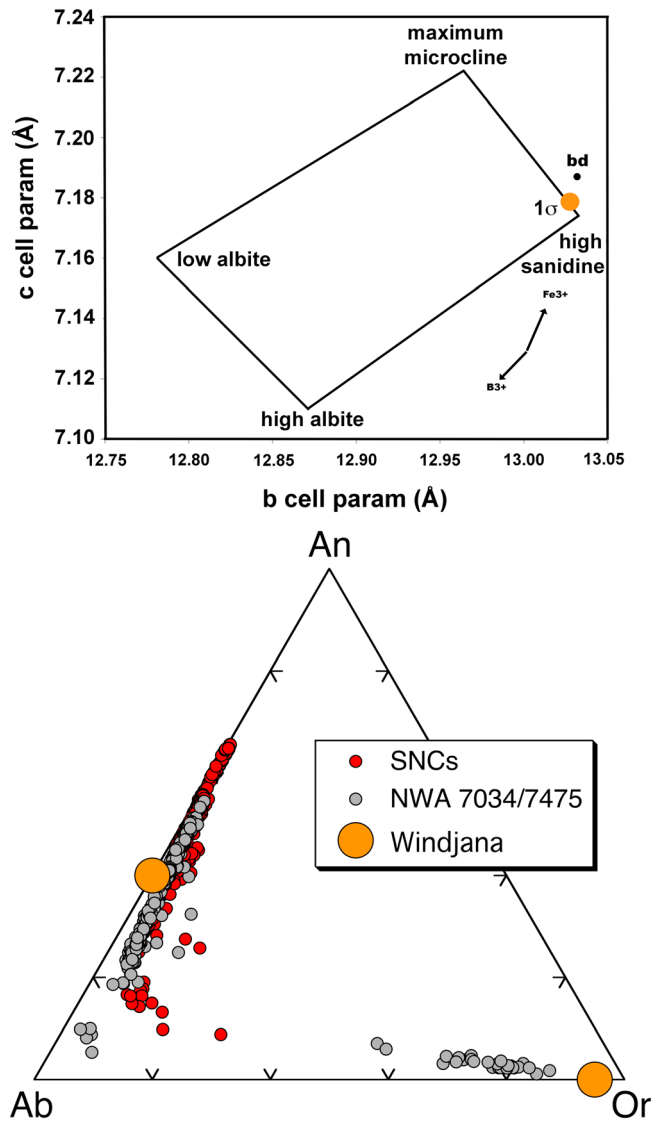


**Figure 5.** Alkali feldspar in Windjana. (a) Unit cell *b-c* plot for alkali feldspars after Wright and Stewart [1968] and Cerny and Chapman [1986]. Circle shows the  $1\sigma$  uncertainty ellipse in the *b-c* cell parameters of the Windjana alkali feldspar (Table 1). Dot “bd” shows cell parameters for buddingtonite,  $(\text{NH}_4)\text{AlSi}_3\text{O}_8$ ; arrows show vectors for substitutions, into high sandine, of  $\text{B}^{3+}$  (reedmergnerite component,  $\text{NaBSi}_3\text{O}_8$ ) and  $\text{Fe}^{3+}$  ( $\text{NaFe}^{3+}\text{Si}_3\text{O}_8$  component). (b) Compositions of the Windjana alkali feldspar and plagioclase compared to feldspars of the SNC Martian meteorites and the NWA 7034 Martian meteorite (and pairs); data from the literature, full reference list on request. Chemical components are as follows: Or,  $\text{KAlSi}_3\text{O}_8$ , Ab,  $\text{NaAlSi}_3\text{O}_8$ ; and An,  $\text{CaAl}_2\text{Si}_2\text{O}_8$ . Windjana sanidine and andesine are plotted as 0% An and 0% Or, respectively, because we lack constraints on those components.

[Martin, 1971]; its cell parameters are  $b = 12.373 \text{ \AA}$  and  $c = 6.808 \text{ \AA}$ . Sanidine rich in  $\text{Fe}^{3+}$  is known from extrusive alkaline igneous rocks [Taroev et al., 2008]; the cell parameter for pure  $\text{KFe}^{3+}\text{Si}_3\text{O}_8$  are  $b = 13.13 \text{ \AA}$  and  $c = 7.347 \text{ \AA}$ . The *b-c* cell parameters of the Windjana alkali feldspar could be replicated by mixtures of these nominally minor components (e.g., both  $\text{B}^{3+}$  and  $\text{Fe}^{3+}$ ) [Cerny and Chapman, 1986], but the simplest explanation is that the Windjana alkali feldspar contains neither  $\text{B}^{3+}$  nor  $\text{Fe}^{3+}$  and is nearly pure  $\text{KAlSi}_3\text{O}_8$ . This is consistent with ChemCam analyses at Windjana (and elsewhere in Gale Crater) that show concentrations of boron essentially at the detection limit (several hundred parts per million; R. C. Wiens, personal communication, 2015). There is

content of very K-rich feldspars [Kroll and Ribbe, 1983]. Given this insensitivity, we infer that the composition of the Windjana alkali feldspar is approximately  $\text{Or}_{95\pm 2}\text{Ab}_{5\pm 2}$  ( $1\sigma$  uncertainty). Structurally, the Windjana alkali feldspar is sanidine (i. e., high K spar) and within uncertainty of having its  $\text{Al}^{3+}$  fully disordered among the possible sites [Kroll and Ribbe, 1987]. Figure 5b compares this composition ( $\text{Or}_{95}\text{Ab}_5$ ) to feldspars that have been analyzed from the SNC meteorites [Papike et al., 2009] and from the polymict breccia NWA 7034/7475 [Santos et al., 2015; Wittmann et al., 2015].

With CheMin data, we cannot evaluate other chemical substitutions in the Windjana sanidine (e.g.,  $\text{B}^{3+}$ ,  $\text{Fe}^{3+}$ ,  $\text{NH}_4^+$ ,  $\text{Ba}^{2+}$ ); given the close match between its *b* and *c* parameters and those of nominal pure sanidine, none of them are likely to be significant. Feldspars with significant  $\text{NH}_4^+$ , the buddingtonite component, are known on Earth in some high-temperature metasomatic deposits and in some sedimentary phosphate deposits; the cell parameters for buddingtonite fall slightly outside the quadrilateral of Figure 5 ( $b = 13.032 \text{ \AA}$ ,  $c = 7.187 \text{ \AA}$ ) but near the sanidine and orthoclase end-members. It seems doubtful that CheMin data alone could distinguish buddingtonite from pure sanidine, but the high abundance of K in the bulk rock analysis (Table 3) and the lack of significant high-temperature evolution of N species during SAM EGA analysis of Windjana [Stern et al., 2015a, 2015b] suggest that its alkali feldspar contains little if any  $\text{NH}_4^+$ .

Other substituents have cell parameters that fall far from the quadrilateral on Figure 5. The  $\text{B}^{3+}$  feldspar, reedmergnerite, occurs in authigenic deposits in B-rich saline environments

no published evidence for significant proportions of any of these substituents in alkali feldspars in the Martian meteorites [Papike *et al.*, 2009; Santos *et al.*, 2015; Wittmann *et al.*, 2015].

### 3.2.2. Plagioclase Feldspar

The Windjana sandstone contains little plagioclase, only ~3% of the crystalline mass (Table 2) compared to ~40% of the Rocknest soil drift [Blake *et al.*, 2013] and ~30% of the mudstones of Yellowknife Bay [Vaniman *et al.*, 2014]. Because the abundance of plagioclase is low and most of its diffraction peaks overlap with those of more abundant phases, its cell parameters and inferred composition are relatively uncertain. Three independent Rietveld refinements yielded essentially the same cell parameters, and their average is in Table 2. Other refinements yielded a wide range of parameters, which is reflected in the cell parameters' large uncertainties, which are given as 1 standard deviation on all of the refined cell parameters (Table 2).

The unit cell parameters of natural plagioclases, at least those between albite (An<sub>0</sub>-10) and labradorite (~An<sub>60</sub>), are simple monotonic functions of chemical composition [Ribbe, 1975]. The most definitive of the cell parameters are the *c* cell length and the angle  $\gamma$ , which range from 7.160 Å and 87.7° for albite (NaAlSi<sub>3</sub>O<sub>8</sub>) to 7.105 Å and 90.1° for andesine/labradorite (Ca<sub>0.5</sub>Na<sub>0.5</sub>Al<sub>1.5</sub>Si<sub>2.5</sub>O<sub>8</sub>); an individual refinement's uncertainty on *c* and  $\gamma$  are ~0.05 Å and 0.3°, which allows some rough specificity of plagioclase composition. The three similar refinements of cell parameters are consistent with a plagioclase composition of ~An<sub>40</sub>, with a standard deviation of the mean of 5 An number (i.e., An<sub>35</sub>-An<sub>45</sub>). If one takes the more conservative uncertainties on individual refinements or on the mean of all refinements, uncertainties in the composition are larger. This plagioclase composition is also plotted on Figure 5b—it falls within the range of compositions found in SNC meteorites [Papike *et al.*, 2009] and in NWA 7034/7475 [Santos *et al.*, 2015; Wittmann *et al.*, 2015].

### 3.2.3. Mafic Silicates

Augite is the most abundant mafic silicate in Windjana, accounting for ~26% of its crystalline material (Table 2). The unit cell parameters of augite are strongly dependent on its chemistry, at least its ratios of “pyroxene quadrilateral” cations Mg, Fe, and Ca [Morrison *et al.*, 2015]. Using those calibrations, the Windjana augite (Table 1) is consistent with a subcalcic augite of composition ~Wo<sub>37</sub>En<sub>42</sub>Fs<sub>21</sub>, (Figure 6a), with uncertainties of ~05 in each of the components and Mg# = 0.68. With CheMin data alone, there is no way to determine abundances of “nonquadrilateral” cations (e.g., Al, Ti, Na, Cr) in the Windjana augite.

Pigeonite is moderately abundant in Windjana, ~15% of the crystalline material (Table 2). Its composition is approximately Wo<sub>05</sub>En<sub>63</sub>Fs<sub>32</sub>, Mg# = 0.66 (Table 1 and Figure 6a) [Morrison *et al.*, 2015], again with uncertainties of ~05 in the En and Fs components. The CheMin data provide no constraints on minor element abundances in the pigeonite. Figure 6 shows that the Gale Crater pyroxene compositions are consistent, in terms of their Ca, Mg, and Fe values, with pyroxenes in the Martian meteorites.

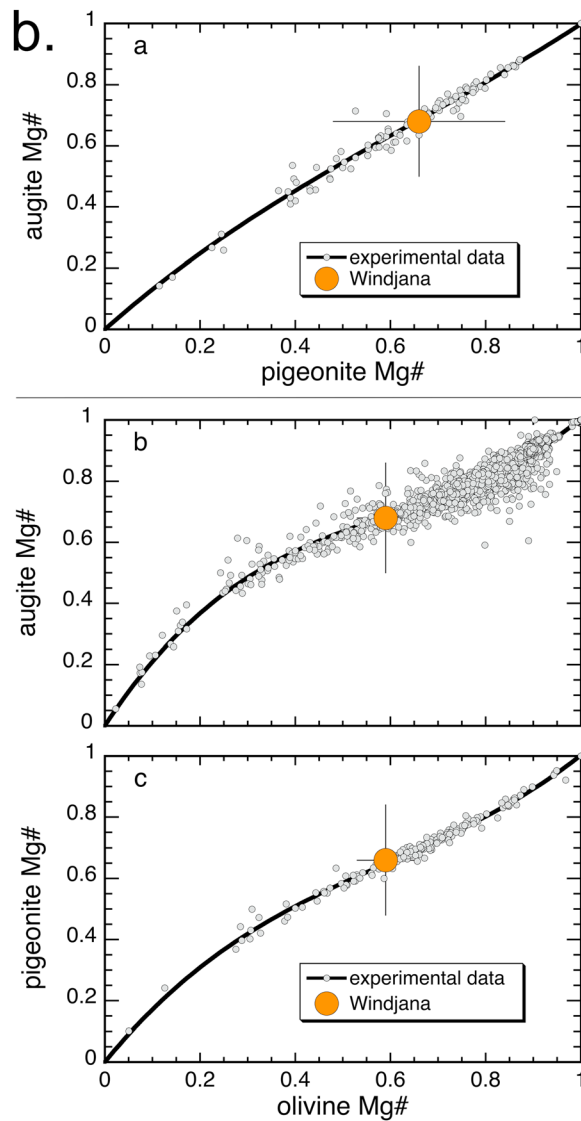
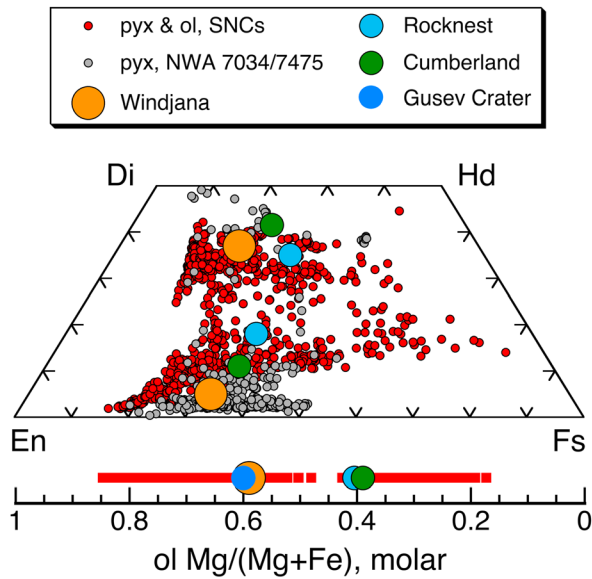
The Windjana sample contains ~6% olivine (by mass) in its crystalline component (Table 2), much less than the 21% in the Rocknest soil drift [Blake *et al.*, 2013] but significantly more than the 2–4% in the Yellowknife Bay mudstones [Vaniman *et al.*, 2014]. From its unit cell volume (Table 1), the Windjana olivine is Fe-forsterite, ~Fo<sub>59±06</sub> with 1 $\sigma$  uncertainties [Morrison *et al.*, 2015]; this composition (Figure 6a) is more magnesian than those inferred for olivine in the Rocknest and Yellowknife Bay materials in Gale Crater [Bish *et al.*, 2013; Vaniman *et al.*, 2014], comparable to that inferred for a Gusev Crater basalt [Filiberto *et al.*, 2008; Morris *et al.*, 2004], and within the very broad range found in the Martian meteorites (Figure 6a) [see Filiberto and Dasgupta, 2011; Papike *et al.*, 2009; Shearer *et al.*, 2008].

The chemical compositions of Windjana's augite, pigeonite, and olivine are consistent with chemical equilibrium at high temperature (Figure 6b), at least with respect to Fe/Mg. This concordance is consistent with the minerals all coming from the same protolith, although a single protolith is not required. This igneous protolith is most likely to be basaltic.

Enstatite (orthopyroxene) is not definitively detected in the Windjana sample. Of the six independent Rietveld refinements, one derived ~3% enstatite in the crystalline mass, while the others refined its abundance to zero (Table 2). If enstatite is present, it is at or below the CheMin detection limit.

### 3.2.4. Iron Oxide Spinel

Iron oxide spinel is relatively abundant in the Windjana sandstone, at ~16% mass of the crystalline material and 12% mass of the whole rock. (Table 2). Because the spinel is cubic, CheMin can retrieve only limited constraints on the composition and cation ordering in a spinel—only the *a* cell dimension, and relative intensities of the



spinel's diffraction peaks. Thus, CheMin data alone cannot retrieve the complex composition of a real spinel, e.g., which could contain significant Ti, Cr, Al, and Mg in addition to Fe [Gattacceca *et al.*, 2014]; however, CheMin data can place significant limits on the range of possible spinel compositions. Beyond that, consideration of other data from the Curiosity rover restricts the spinel to being magnetite proper, with very little excess Fe<sup>3+</sup> accommodated by site vacancies (maghemite component) and/or Ti (ulvöspinel component), and some small proportion of Al and/or Mg (hercynite and magnesioferrite components).

**3.2.4.1. Constraints From Unit Cell Parameter**

The *a* cell parameter for the Windjana spinel is  $a = 8.389 \pm 0.006 \text{ \AA}$  (Table 1), the mean value and 1 standard deviation of the Rietveld refinements. The uncertainty on the precision of each

**Figure 6.** Mafic mineral compositions in the Windjana sample. (a) Figure 6. (pyx and ol Windjana *et al.*\_11-18-15) Compositions of bulk pyroxenes (pyx) estimated by CheMin refinement for the Gale Crater samples Windjana (this study) and Rocknest and Cumberland [Morrison *et al.*, 2015] projected onto the pyroxene quadrilateral (molar). Also plotted are pyroxene compositions from 19 SNC meteorites [Papike *et al.*, 2009] and from NWA 7034/7475 [Santos *et al.*, 2015; Wittmann *et al.*, 2015]. Estimated bulk olivine (ol) compositions from Windjana, Rocknest, and Cumberland, samples are plotted as a function of Mg/(Mg + Fe), molar below the pyroxene quadrilateral. Also plotted is the estimated olivine composition at Gusev Crater [Morris *et al.*, 2004] and olivine compositions from selected SNC meteorites [Papike *et al.*, 2009]. (b) Estimated Mg#s based on bulk compositions of augite, pigeonite, and olivine from the Windjana sample (this study) compared to coexisting pyroxenes and olivines in low to high-pressure experiments. Solid black line in each panel is a third-order polynomial least squares fit to the experimental data. (top) Augite Mg# versus pigeonite Mg#; (middle) augite Mg# versus olivine Mg#; (bottom) pigeonite Mg# versus olivine Mg#; where Mg# = Mg/(Mg + Fe), molar. See the supporting information for the reference list for the experimental data.

individual refinement is  $\sim 0.002 \text{ \AA}$ , which is consistent with the uncertainty on the mean value. As noted above, the accuracy of cell parameters may be worse than this because of uncertainty in the distance between analysis cell and X-ray detector. This  $a$  value is smaller than that of pure stoichiometric magnetite,  $\text{Fe}_3\text{O}_4$ , which has  $a = 8.3961 \pm 0.0007 \text{ \AA}$  [Okeruda, 1997; Wechsler et al., 1984], and that difference can be interpreted in terms of the spinel's chemical composition. Many substituents into  $\text{Fe}_3\text{O}_4$  can reduce its unit cell dimension to that observed in the Windjana sandstone. The most likely in reasonable geological settings include chromium, ferric iron, magnesium, and aluminum, which can be represented as solid solutions toward the spinel end-members: chromite ( $\text{FeCr}_2\text{O}_4$ ),  $a = 8.3765 \text{ \AA}$ ; maghemite ( $\gamma\text{-Fe}_2\text{O}_3$ ),  $a = 8.34 \text{ \AA}$ ; magnesioferrite ( $\text{MgFe}_2\text{O}_4$ ),  $a = 8.38\text{--}8.340 \text{ \AA}$ , depending on ordering state; and hercynite ( $\text{FeAl}_2\text{O}_4$ ),  $a = 8.152 \text{ \AA}$  [Antao et al., 2005; Golla-Schindler et al., 2005; Gorski and Scherer, 2010; Hamecher et al., 2013; O'Neill et al., 1992]. The Windjana spinel is likely a complex solid solution of these (and other) components or end-members, but CheMin data cannot distinguish among them. So we consider here only binary solid solution series.

First, it would be reasonable for the Windjana magnetite to be a solid solution toward chromite (or be a physical mixture of magnetite proper and chromite), because chromite and chrome spinel are common accessory phases in basalts. If the only substituent were chromium, the  $a$  cell parameter (and uncertainty) would be consistent with composition ranges of  $\text{Mt}_{80}\text{Chr}_{20}$  to  $\text{Mt}_{62}\text{Chr}_{38}$  or  $\sim\text{Mt}_{10}\text{Chr}_{90}$  [Kurepin, 2005; Levinstein et al., 1972]. There are two possible ranges here because the  $a$  cell parameter is a highly nonlinear function of composition along the magnetite-chromite join (the former being an inverse spinel and the latter a normal spinel).

It would also be reasonable for the magnetite in Windjana to have been produced diagenetically by oxidation of olivine (as proposed for the Yellowknife Bay mudstones [Bristow et al., 2015; Vaniman et al., 2014]). In that case, one might expect it to contain significant additional  $\text{Fe}^{3+}$  as maghemite component (i.e., cation-deficient magnetite), but not Cr. In that case the Windjana magnetite would be consistent with a composition between  $\text{Fe}^{2+}/\text{Fe}^{3+} = 0.35\text{--}0.45$ , i.e.,  $\text{Mt}_{70}\text{Mh}_{30}$  to  $\text{Mt}_{90}\text{Mh}_{10}$  [Gorski and Scherer, 2010; Lilova et al., 2012; Schmidbauer and Keller, 2006].

Aluminum is a common minor substituent in magnetite-rich spinels and can be represented by the hercynite component,  $\text{FeAl}_2\text{O}_4$ . Between magnetite and hercynite, the unit cell parameter  $a$  varies nearly linearly with composition [Golla-Schindler et al., 2005]. From that data, if the Windjana magnetite were solely a solid solution between magnetite and hercynite, its composition would be approximately  $\text{Mt}_{95}\text{Hc}_{05}$ .

Magnesium is also a common minor substituent in magnetite-rich spinels, as the magnesioferrite component,  $\text{MgFe}_2\text{O}_4$ . The  $a$  cell parameter for pure  $\text{MgFe}_2\text{O}_4$  can vary significantly depending on its ordering state, with values near that of the Windjana spinel at the greatest order state (i.e., low-formation temperature,  $<600^\circ\text{C}$ ) [Antao et al., 2005; O'Neill et al., 1992]. So if the Windjana magnetite were solely a solid solution between magnetite and magnesioferrite, it would be very rich in magnesioferrite, in the vicinity of  $\text{Mt}_{25}\text{Mf}_{75}$ . In crustal settings (on Earth), such magnesioferrite-rich spinels are uncommon and found only in highly oxidized, extreme-temperature settings (e.g., impact spherules, meteorite fusion crusts) and in rare carbonatites and igneous rocks [Shi et al., 2009].

Titanium substitution, as in titanomagnetite and the  $\text{ulvospinel}$  component, increases the  $a$  cell parameter [Bosi et al., 2009; Wechsler et al., 1984] and is thus unlikely to be significant in the Windjana magnetite. However, Ti substitution charge balanced by vacancies (as in titanomaghemite) could yield a magnetite with a reasonable  $a$  cell parameter; i.e., a fully oxidized titanomaghemite has  $a = 8.358 \text{ \AA}$  [Allan et al., 1989].

#### 3.2.4.2. Constraints From Diffraction Peak Heights

Although spinel (being cubic) has few diffraction peaks, the relative intensities of those peaks carry some information on the composition and cation distribution of the spinel. From the Windjana pattern, one can readily extract relative intensities of three spinel diffraction peaks: 400 ( $d \approx 2.099 \text{ \AA}$ ); 113 ( $d \approx 2.53 \text{ \AA}$ ); and 111 ( $d \approx 4.85 \text{ \AA}$ ), see Figure 4b. Two other peaks are buried among diffraction from other phases: 222 ( $d \approx 2.43 \text{ \AA}$ ) and 220 ( $d \approx 2.97 \text{ \AA}$ ).

The peak height ratio 111/113 varies significantly among spinels:  $\sim 12\%$  in titanomaghemite [Collyer et al., 1988];  $\sim 10\%$  for chromite;  $\sim 8\%$  for magnetite;  $\sim 3\%$  in maghemite; and  $<1\%$  in pure hercynite (based on measured and synthetic patterns) [Chichagov et al., 2001]. The peak ratio 111/113 for the Windjana spinel is near 8%, as calculated from the observed pattern (subtracting from the apparent 113 peak intensity contributions from the augite  $-131$  peak)—this can be seen qualitatively in the difference curve on

Figure 4b, which is calculated for a noncation-deficient magnetite. There is no significant difference between the observed and fitted patterns over the 111 peak position, implying that the 111/113 intensity ratio in the Windjana spinel is like that of pure magnetite. Thus, the peak ratio would be inconsistent with large proportions of chromite, maghemite, titanomaghemite, and hercynite in the Windjana spinel.

#### 3.2.4.3. Other Constraints and Summary

With CheMin data only, it is not possible to define the composition of the Windjana magnetite, but some compositional ranges are quite unlikely. As described above, CheMin data imply that the Windjana spinel is close to pure magnetite and likely contains little substitutions of Ti or  $\text{Fe}^{3+}$ , the ulvöspinel and maghemite components. The paucity of maghemite component is supported by passive reflectance spectra from the ChemCam instrument on MSL, which are more consistent with a “pure” magnetite [Johnson *et al.*, 2015b].

From CheMin data, the Windjana spinel could contain a moderate to large proportion of the chromite component ( $\text{Mt}_{80}\text{Chr}_{20}$  to  $\text{Mt}_{10}\text{Chr}_{90}$ ), but the bulk rock chemical composition excludes even a moderate constituent of the spinel. A spinel with a composition of  $\text{Mt}_{80}\text{Chr}_{20}$  contains ~13.2 wt %  $\text{Cr}_2\text{O}_3$ . Given that spinel comprises ~12.4% of the Windjana sandstone, such a spinel composition would contribute ~1.6 wt %  $\text{Cr}_2\text{O}_3$  to the bulk rock composition—more than three times the  $\text{Cr}_2\text{O}_3$  content of the Windjana Dump Pile (Table 1). Thus, while we cannot rule out the presence of some chromite as a solid solution component in the spinel, if it is present, its abundance must be quite small, especially since some fraction of the bulk rock  $\text{Cr}_2\text{O}_3$  will be present in the pyroxenes (augites in NWA 7034/7475 and in the SNCs can contain up to ~1 wt %  $\text{Cr}_2\text{O}_3$ ; [Papike *et al.*, 2009; Santos *et al.*, 2015; Wittmann *et al.*, 2015]).

Discounting significant Mg substitution (as magnesioferrite component) as geologically unreasonable, we are left to infer that the Windjana spinel is most likely to be magnetite with a small proportion of Al substitution (~5% molar of hercynite component). This inference is not unique, as we lack data to define or detect small proportions of other substitutions or of complex solid solutions that might mimic this simple result (e.g., a spinel rich in both Ti and Al)—note that most spinels in basaltic igneous rocks contain multiple end-member components [Barnes and Roeder, 2001] and that spinels formed under diagenetic conditions (e.g., ~25°C) can contain significant Al [Schwertmann and Murad, 1990]).

#### 3.2.5. Other Minerals

Ilmenite ( $\text{FeTiO}_3$ ) is present in the Windjana sandstone but only at ~1.1% weight, near the CheMin detection limit (Table 2). Hematite is also present in the Windjana sandstone and also near the CheMin detection limit at ~0.7% mass (Table 2).

Pyrrhotite is the only sulfide mineral detected in the Windjana sandstone; it was detected in three of the six refinements and is near the detection limit of ~0.4% by mass of the crystalline material (Table 2). It is not possible to determine which polytype is present—characteristic minor diffractions (as for superstructures) are not visible above the background, and the unit cell parameters of the pyrrhotite are not characteristic of a specific polytype.

Akaganeite [ $\beta\text{-FeO}(\text{OH,Cl})$ ] is present in the Windjana sandstone at the detection limit of ~0.3% by mass (Table 2). Its unit cell parameters are distinctive for the mineral but not particularly informative about its composition, notably its proportion of Cl. The unit cell parameters (Table 1) are perhaps more consistent with Cl-rich akaganeite rather than OH rich [Takagi *et al.*, 2010]. However, little more can be said in the absence of more precise cell parameters for the Windjana akaganeite and additional laboratory data.

Fluorapatite [ $\text{Ca}_5(\text{PO}_4)_3\text{F}$ ] is almost certainly present in the Windjana sandstone, although its detection by CheMin is not entirely definitive. Four of the six Rietveld refinements detected fluorapatite (2.5, 1.0, 0.5, and 1.1% mass), and the abundance of  $\text{P}_2\text{O}_5$  in the APXS chemical analysis of the sandstone (Table 3) is consistent with ~1% apatite. Fluorine has been detected in the Windjana sandstone by ChemCam LIBS [Forni *et al.*, 2015], lending further credence to the presence of fluorapatite.

Anhydrite ( $\text{CaSO}_4$ ) is present in the Windjana sandstone, although essentially at detection limit (Table 2); its refined cell parameters are distinctive for the phase but not otherwise informative. Bassanite ( $\text{CaSO}_4 \cdot 0.5\text{H}_2\text{O}$ ) is not definitively present—four of the six Rietveld refinements gave ~1% bassanite, but the remaining two gave zero.

Minor jarosite is possible in the Windjana sandstone, but it was not detected definitively as it was at Terra Meridiani [Squyres and Knoll, 2005]. One of the Rietveld refinements converged to 0.8% weight of jarosite, but it was not detected (or refined to zero abundance) in the others. If present, jarosite's abundance in the Windjana rock is at or below CheMin's detection limit.

### 3.2.6. Not Detected

Many minerals that are characteristic of specific geochemical processes are definitely not present in the Windjana sandstone at the CheMin detection limits. In particular, no products of hydrothermal alteration have been detected, such as might have been produced in an impact-induced hydrothermal system [Schwenzer *et al.*, 2012; Schwenzer and Kring, 2013]. Nor has CheMin detected (at the percent mass level) soluble salts such as sulfates, halides, and perchlorates [Chipera and Vaniman, 2007; Farrand *et al.*, 2014; Forni *et al.*, 2015; Johnson *et al.*, 2015b]. CheMin's nondetection of carbonate minerals is consistent with the results of SAM evolved gas analysis. Some of the CO<sub>2</sub> detected during SAM EGA likely derives from oxidation of organic material (e.g., from the SAM background) by O<sub>2</sub> released from oxychlorine phases in the sample, based on its near-coincidence with a peak in release of O<sub>2</sub> [McAdam *et al.*, 2015]. Part of the CO<sub>2</sub> detected could also derive from thermal decomposition of Fe carbonates [Sutter *et al.*, 2015], but the abundance of carbonate implied by this CO<sub>2</sub> would be below CheMin detection limits.

### 3.3. Poorly Crystalline Components

Approximately 25% of the Windjana sandstone is poorly crystalline or amorphous, which appears in X-ray diffraction as broad "peaks" or humps. From the shapes and locations of those features, three of the contributions can be assigned to phyllosilicates and two contributions to amorphous materials.

#### 3.3.1. Phyllosilicates

The Windjana diffraction pattern shows two features consistent with 001 diffractions from 2:1 phyllosilicate minerals: a moderately sharp peak at 10.1° 2 $\theta$  and low broad peak or band from ~7° 2 $\theta$  to ~12° 2 $\theta$  (Figure 4b). The sharper peak gives a  $d$  spacing of ~10.2 Å, which is consistent with the 001 diffractions of illite, collapsed nontronite, or a collapsed ferromagnesian smectite. However, the 001 diffraction of the inferred collapsed smectite of the John Klein drill sample (Yellowknife Bay) is much broader than that in the Windjana sample [Bristow *et al.*, 2015; Vaniman *et al.*, 2014], and the Griffith Park ferromagnesian smectite used as an analog to the clays at Yellowknife Bay collapses only to 001 of 11.8 Å [Treiman *et al.*, 2014]. The broad low peak or band is very similar to the smectite diffraction "hump" in the John Klein drill sample from Yellowknife Bay [Bristow *et al.*, 2015; Vaniman *et al.*, 2014], which is interpreted to represent a collapsed (dehydrated) ferromagnesian smectite, possibly with chloritic interstratifications. For the Windjana sample, we lack diffraction data on treated samples that would normally be used to distinguish among illite, nontronite, and smectite. By analogy with other Gale Crater samples, we infer that the phyllosilicates are dominantly collapsed smectites [Vaniman *et al.*, 2014]. The presence of illite or illitic interstratifications cannot be disproven, but (as shown later) the chemical composition of the amorphous and clay material includes very little Al or K, and thus little illite component. The mass abundance of the phyllosilicates (sharp peak and broad band) was determined by FULLPAT analysis (Table 2) [Chipera and Bish, 2002].

The Windjana X-ray diffraction pattern shows a low broad peak at ~14° 2 $\theta$  (Figure 4b), which suggests a small proportion of ~7 Å 1:1 phyllosilicate mineral. This peak refined to a  $d$  spacing of ~7.15 Å, which is consistent with kaolinite and less so with the serpentine minerals (which have 001  $d$  spacings at ~7.25 Å). This phase is present at the CheMin detection limit—the peak area refines to ~1% by mass of the total sample during Rietveld analysis with the well-crystalline phases (Table 2). No other peaks assignable to kaolinite are above background and distinct from interferences from other minerals' diffractions. Kaolinite is a reasonable identification for this diffraction peak, as it is a common product of low-temperature hydrous alteration of alkali feldspar.

#### 3.3.2. Amorphous

The Windjana sandstone contains a significant proportion of X-ray-amorphous material, which is apparent in the diffraction pattern (Figure 4b) as both the strong rise in background below ~7° 2 $\theta$  and a hump in the background level between ~15° to 45° 2 $\theta$ , centered at ~30° 2 $\theta$ . The rise low 2 $\theta$  is consistent with a phase like hisingerite or allophane (as suggested for similar features in X-ray diffraction patterns of the Yellowknife Bay mudstones [Vaniman *et al.*, 2014]) and with some samples of ferrihydrite. The broad background hump, centered at ~30° 2 $\theta$ , is consistent with several types of amorphous material, including silicate glass and iron oxyhydroxides (similar to ferrihydrite) [Bish *et al.*, 2013; Morris *et al.*, 2013]. The mass of the amorphous material (Table 2) was determined by FULLPAT analysis [Chipera and Bish, 2002]. In the discussion below, we constrain the bulk composition of the amorphous components (following the approach of Dehouck *et al.* [2014]) and then use the calculated bulk composition to infer possible constituents.

## 4. Interpretation and Discussion

### 4.1. Poorly Crystalline and Amorphous Material

Amorphous and poorly crystalline components comprise significant fractions of the materials analyzed by CheMin in Gale Crater [Bish *et al.*, 2013; Blake *et al.*, 2013; Vaniman *et al.*, 2014], and the Windjana sandstone is no exception (Table 2). One can calculate the chemical composition of the amorphous and poorly crystalline material from the bulk composition of the rock and the proportions and compositions of the crystalline phases (Tables 1 and 2, see text above). However, the CheMin data do not provide sufficient constraints to uniquely determine the natures and compositions of these poorly crystalline constituents. Here we propose a model of the amorphous and poorly crystalline components that is generally consistent with Windjana's elemental composition, CheMin data, and geochemical setting; this model is not unique.

The elemental composition of the Windjana sandstone was analyzed by the APXS instrument [Gellert *et al.*, 2014a, 2014b]; analytical targets included: the unbrushed rock surface, the surface brushed clear of dust by the DRT (Dust Removal Tool), tailings from the main drill hole, and sieved drill powder dumped from CHIMRA (Table 3). The dumped material is the remainder of the sieved sample, after aliquots were portioned and delivered to the CheMin and SAM instruments. The unbrushed surface of the Windjana sandstone is clearly distinct from the brushed and internal samples (Table 3), being richer in elements characteristic of Mars' windblown dust like S and Cl [Ming *et al.*, 2008; Yen *et al.*, 2005]. The brushed surface still contains more S and Cl than the drilled (interior) samples, suggesting that some dust remains on the surface. The drilled samples (the tailings and the CHIMRA dump) are not identical, which likely represents real variability of the Windjana sandstone composition. The tailings samples include more material from near the rock's surface than its interior, suggesting that the surface of Windjana is enriched in K and Cl, and depleted in Ca, Fe, and S compared to its interior (Table 3). In any case, we assume that the CHIMRA dump sample represents the material analyzed by CheMin.

#### 4.1.1. Chemical Composition of "Amorphous" Material

To calculate the composition of the poorly crystalline and amorphous material in the Windjana sandstone, we subtract the material of the CheMin-determined crystalline fraction (mineral proportions and compositions) from the APXS composition of the dump sample. Uncertainties on all analyses are carried through the calculation, which is done using a Monte Carlo method; see the supporting information for details and a spreadsheet of the calculation. The calculated composition of the Windjana amorphous and poorly crystalline material (amorphous + phyllosilicates) is given in Table 3. That composition is notable for its high abundances of Fe and Mg, correspondingly low abundance of SiO<sub>2</sub>, and high abundances of SO<sub>3</sub> and Cl.

It is significant that the calculated composition of the amorphous and poorly crystalline material shows, within uncertainties, no negative oxide abundances and near-zero abundances of K<sub>2</sub>O, P<sub>2</sub>O<sub>5</sub>, and CaO. These observations imply that the CheMin results for mineral proportions and compositions are consistent with the APXS chemical analyses. Further, it appears that all the K<sub>2</sub>O in Windjana is contained in its sanidine, that all the P<sub>2</sub>O<sub>5</sub> is in apatite, and that CheMin has missed no Ca-bearing phases. The nominal K<sub>2</sub>O abundance in the amorphous and poorly crystalline material is negative, although within uncertainty of zero; the nominal abundance of K<sub>2</sub>O would be zero if Windjana contained ~19% of Or<sub>95</sub> alkali feldspar, which is within uncertainty of the nominal CheMin abundance of 21 ± 3% 1σ (Table 2). All of the P<sub>2</sub>O<sub>5</sub> in the Windjana APXS analysis would be explained by 1.7% fluorapatite, compared to the nominal CheMin abundance of 1.1 ± 1.0% 1σ (Table 2). We take these concordances as evidence that the CheMin and APXS analyses are consistent with each other and are of the same material (Table 3) and that the CheMin refinements represent accurately the mineral proportions of the Windjana sample.

#### 4.1.2. A Model

Collectively, the amorphous and poorly crystalline materials in Windjana produce four distinct contributions to the CheMin XRD pattern: a broad and a sharp diffraction peak both centered at ~10° 2θ, strong intensity at low 2θ, and a broad hump between 15 and 45° 2θ (Figure 4b). One would like to constrain the chemical compositions of these components, but the calculation is severely underdetermined. Here we propose a model for the natures and compositions of these components, informed by geological constraints from the rock itself and what is known from other rocks at Gale Crater.

Our model for these components starts with the calculated bulk composition (Table 3), from subtracting the compositions of the crystalline phases (weighted by their mass fractions) from the bulk rock composition. In



the “amorphous + poorly crystalline” compositions, abundances of several elements must be overestimates because of our limited constraints on the true compositions of the crystalline phases. The calculated  $\text{TiO}_2$  and  $\text{Cr}_2\text{O}_3$  contents of the amorphous + poorly crystalline components are certainly overestimates, because (1)  $\text{TiO}_2$  and  $\text{Cr}_2\text{O}_3$  in Martian pyroxenes can be as high as ~2 and 1 wt %, respectively [Papike *et al.*, 2009; Santos *et al.*, 2015; Wittmann *et al.*, 2015], and our calculation assumed 0 wt % for both; and (2) we assumed (as discussed above) that the spinel phase is essentially pure magnetite, although it could reasonably contain small proportions of Ti and Cr. Similarly, the calculated  $\text{Al}_2\text{O}_3$  and  $\text{Na}_2\text{O}$  contents of the amorphous + poorly crystalline components are certainly overestimates, because  $\text{Al}_2\text{O}_3$  and  $\text{Na}_2\text{O}$  can be as high as 6–7 and ~0.6 wt %, respectively, in Martian pyroxenes, and our calculation assumes 0 wt % for both.

Then, we assign elements in the amorphous + poorly crystalline material to likely chemical components. First, approximately a third of this material should be clay minerals (Table 2). Those clay minerals can include little illite because all the  $\text{K}_2\text{O}$  in the Windjana whole rock is accounted for by its alkali feldspar; so we assume that the clay is all smectite/saponite as with the Yellowknife Bay rocks [Bristow *et al.*, 2015; Vaniman *et al.*, 2014]. We can assign Na to Cl (chloride, chlorate, or perchlorate) and MgO and the little remaining CaO to  $\text{SO}_3$ , assuming charge balance and that these components are present as poorly crystalline sulfate materials. The remaining amorphous + poorly crystalline material has molar  $(\text{Mg} + \text{Fe} + \text{Mn})/(\text{Si} + \text{Al})$  far in excess of that for smectite, so we assign all the Si and Al (what little there is) and a proportional amount of the Mg and Mn to the clay mineral. This subtraction leaves a significant proportion of Fe and Mg unassigned to silicate or ionic components. We can suggest two possible hosts for the excess Mg: the amorphous material contains a component of  $\text{Mg}(\text{OH})_2$ , brucite; or the smectite is partially chloritized. These explanations are chemically equivalent, as chlorite minerals consist of smectite-like layers alternating with brucite layers [Bailey, 1988]. Brucite is potentially reasonable, as it can be formed during aqueous alteration of olivine [O’Hanley, 1996]; partially chloritized smectite has been invoked to explain the XRD properties of clays in the Yellowknife Bay area of Gale Crater [Bristow *et al.*, 2015].

Allophane and/or hisingerite have been proposed as phases in the Windjana sandstone (and other materials of Gale Crater) to account for the sharp rise in diffracted intensities at  $2\theta < 10^\circ$  [Bish *et al.*, 2013; Rampe *et al.*, 2012]. However, the calculated bulk composition of the amorphous material in Windjana is not consistent with these inferences. Allophane is “a poorly-crystalline, hydrous aluminosilicate ... with short-range crystallographic order and molar Si/Al ratios ranging from ~0.5 to 1” [Bish *et al.*, 2013; Rampe *et al.*, 2012], but it cannot be abundant in the Windjana sandstone because the amorphous and poorly crystalline components contain little Al (Table 3) [Morris *et al.*, 2013]. Hisingerite is a ferric iron analog to allophane, again with molar Si/Fe ratios of ~0.5 to 1; it has a nominal composition between  $\text{Fe}_2^{3+}\text{SiO}_5 \cdot 2\text{H}_2\text{O}$  and  $\text{Fe}_2^{3+}\text{Si}_2\text{O}_5(\text{OH})_4 \cdot 2\text{H}_2\text{O}$  [Dehouck *et al.*, 2014; McAdam *et al.*, 2014]. The amorphous and poorly crystalline materials contain abundant iron but not enough silica left over after allocation to smectite to allow a significant proportion of hisingerite.

Iron accounts for the bulk of remaining unassigned elements in Windjana’s amorphous material, and it must be assigned to iron oxides and/or hydroxides [see Morris *et al.*, 2013]. Some of the sulfur could have been assigned to a jarosite mineral or component in the amorphous material (jarosite was detected in one of the Rietveld refinements). Presence of a sulfate component in the amorphous material is confirmed by SAM evolved gas analysis, which yielded more  $\text{SO}_2$  than can be attributed to the pyrrhotite and possible jarosite detected by CheMin (the Ca sulfates detected by CheMin are not expected to decompose in the SAM temperature range) [McAdam *et al.*, 2015]. The bulk of the so-far unassigned iron could be present as nanophase (poorly diffracting) hematite and/or magnetite, ferrihydrite (approximately  $\text{Fe}_2^{3+}\text{O}_3 \cdot 0.5\text{H}_2\text{O}$ ), or the ferric-ferrous iron substances like “green rust.” The latter are double-layer hydroxide phases, like  $\text{Fe}_2^{3+}(\text{Fe}^{2+}, \text{Mg})_6(\text{OH})_{18} \cdot 4\text{H}_2\text{O}$ , some of which contain anions besides  $\text{OH}^-$ , e.g., fougérite,  $\text{Fe}_4^{2+}\text{Fe}_2^{3+}(\text{OH})_{12}\text{CO}_3 \cdot 3\text{H}_2\text{O}$ , and  $\text{Fe}_4^{2+}\text{Fe}_2^{3+}(\text{OH})_{12}\text{SO}_4 \cdot 3\text{H}_2\text{O}$ . Of these, some ferrihydrite samples show strong diffraction intensity at low  $2\theta$  values [e.g., Parfitt *et al.* 1992; Schwertmann *et al.* 1999] and also are consistent with the amorphous hump peaking around  $30^\circ 2\theta$  (Figure 4b). The inference of hydrous poorly ordered iron-rich components is consistent with SAM evolved gas results for Windjana; the observed broad water release from ~100 to 450°C is consistent with laboratory SAM-like EGA analyses of such phases [McAdam *et al.*, 2015]. Thus, we infer the presence of ferrihydrite or similar iron-rich phase from the CheMin XRD and APXS bulk composition of Windjana.

To summarize, constraints from chemistry and X-ray diffraction suggest that the amorphous and poorly crystalline materials in the Windjana sandstone consist of several components. The silica and most of the

magnesia can be assigned to a magnesian smectite; the remaining magnesia is paired with the sulfur as a  $\text{MgSO}_4 \cdot n\text{H}_2\text{O}$  component in the amorphous material. Most of the Fe must be present as poorly diffracting oxide and/or hydroxides, like ferrihydrite. There can be little allophane or hisingerite present, and there is no evidence for Mn-rich phases [Le Deit *et al.*, 2015]. Similarly, there is no evidence that the amorphous component of Windjana contains a significant proportion of igneous or impact glasses. The chemical composition of the amorphous material in Windjana is distinctly different from the estimates of Dehouck *et al.* [2014] for the amorphous components in the Rocknest, Cumberland, and John Klein samples. Dehouck *et al.* [2014] found that those amorphous materials were far richer in  $\text{SiO}_2$  and poorer in MgO and FeO than for Windjana (Table 3); it is not clear how these various amorphous components could be related.

## 4.2. Diagenesis and Cement

The Windjana sandstone experienced some diagenetic alteration, which is expressed in its mineralogy and was obviously cemented in that it is a solid rock (and not loose sand grains). Away from the Windjana site itself, the Dillinger member shows clear evidence of diagenesis by the presence of Mn-rich fracture fillings or surfaces [Lanza *et al.*, 2014] and diagenetic concretions [Grotzinger *et al.*, 2015b]. However, diagenesis (beyond this cementation) of the Windjana sample was limited because it still contains significant proportions of easily altered minerals, notably olivine, plagioclase feldspar, and pyrrhotite.

### 4.2.1. Iron Oxide Cement

Most of the sedimentary rocks examined by Curiosity are rich in iron; many contain ~20% FeO (by APXS), and the extreme (before the Windjana analysis) was the Et\_Then rock with 26.3% FeO equivalent (all Fe calculated as FeO) [Schmidt *et al.*, 2014b]. The Windjana sample is even richer in iron with 27.6% FeO equivalent (Table 3)—the iron is present both as magnetite ( $\text{Fe}_3\text{O}_4$ ) and as poorly diffracting oxides/hydroxides in the amorphous material (see above).

These high FeO abundances are far greater than those expected from sediments and sedimentary rocks of basaltic parentage [Blake *et al.*, 2013; Vaniman *et al.*, 2014] and so have been ascribed to iron-rich cements [Anderson *et al.*, 2015b; Blaney *et al.*, 2014; Grotzinger *et al.*, 2014; Schmidt *et al.*, 2014a; Wiens and Maurice, 2015]. The Windjana sample, being Fe-rich like the other sedimentary rocks of Gale Crater, provides an opportunity to test the hypothesis of iron-rich cements. In the Windjana sample, potential iron-rich cement materials are its magnetite (12% by mass, Table 3) and its amorphous material (~15%), which as discussed above is likely to be Fe-O-(H) material like ferrihydrite or “green rust.” Lesser proportions of the iron are in augite, pigeonite, and olivine; and still smaller proportions in ilmenite, hematite, akaganeite, and pyrrhotite.

It seems reasonable that the Windjana rock is cemented by its magnetite and Fe-rich amorphous material. First, the mass proportions of these phases together, ~27%, represents a volume proportion of ~30–35%, which is reasonable for the porosity of silt or sand sediment [Freeze and Cherry, 1979]. Second, the magnetite is most likely to be nearly pure  $\text{Fe}_3\text{O}_4$ , possibly with some Al substitution (see above), which is inconsistent with an igneous origin (i.e., no evidence of Cr or Ti substitutions) but is consistent with formation at Mars ambient temperatures [Schwertmann and Murad, 1990]. Third, diagenetic, amorphous Fe-O-(H) material is known as a cement in basaltic and in pedogenic systems on Earth. And, fourth, decomposition products of Fe-O-(H) material, including a magnetite-like spinel phase, are present in the matrix of the NWA 7034 Martian meteorite [Muttik *et al.*, 2014]. Thus, we infer that the Windjana sample was cemented by its magnetite and Fe-O-(H) amorphous material; it seems reasonable to extrapolate this inference to the other Fe-rich rocks in Gale Crater, and this can be tested with combined CheMin and chemical analyses.

### 4.2.2. Phyllosilicate

The Windjana sample contains a significant proportion of phyllosilicates, interpreted as smectites and possibly a small proportion of kaolinite (Table 2); there is no evidence for a significant proportion of illite. CheMin data by itself cannot show whether the Windjana phyllosilicates are diagenetic or detrital, but a diagenetic origin seems reasonable in light of a similar inference about smectite in the Yellowknife Bay mudstones [Bristow *et al.*, 2015; Treiman *et al.*, 2014; Vaniman *et al.*, 2014]. As noted above, the Windjana sandstone is well cemented; however, this cement cannot be mechanically strong (e.g., like quartz), because Curiosity's drill penetrated Windjana with relative ease. Cementation by phyllosilicates would satisfy this constraint: there is enough phyllosilicate in Windjana (Table 2) to be such a cement and similar cement has been seen in a basaltic sandstone at Griffith Park, CA (near the locality of Treiman *et al.* [2014], see also Critelli and Ingersoll [1995]).

Although we cannot definitively say that Windjana contains smectite, it would be a reasonable product of aqueous alteration of olivine as hypothesized for the Yellowknife Bay rocks [Bristow *et al.*, 2015; Vaniman *et al.*, 2014] and demonstrated for the Griffith Park saponite [Treiman *et al.*, 2014]. If all the smectite in Windjana formed this way, the original sediment would have contained ~15% olivine rather than the observed 6% (Table 2).

The small proportion of kaolinite in Windjana could reasonably be a diagenetic alteration product of its plagioclase or its alkali feldspar [Garrels and Christ, 1990]. If so the proportions of feldspar in the original sediment would have been slightly greater than presently observed (Table 2). The presence of kaolinite also suggests that a portion of clay mineral material could be illite, as it is an intermediate alteration product between plagioclase and kaolinite [Garrels and Christ, 1990]. CheMin data cannot distinguish illite from smectite, but the calculated bulk composition of the amorphous and poorly crystalline materials has nearly no Al and thus permits little illite.

#### 4.2.3. Other Materials

Akaganéite is present near detection limit in the Windjana sample (Table 2). Akaganéite typically forms on Earth in mildly acidic environments, at low temperatures, from solutions rich in Cl and Fe [e.g., Bibi *et al.* 2011; Cai *et al.* 2001; Holm *et al.* 1983]. Akaganéite is a common alteration product of sulfide minerals, including pyrrhotite [Harries *et al.*, 2013; McLennan *et al.*, 2014]. The pyrrhotite observed in Windjana could be the precursor for its akaganéite, but the fact that pyrrhotite is still present suggests again that diagenesis was relatively minor. Akaganéite has been detected on the Martian surface from orbit [Bishop *et al.*, 2015; Carter *et al.*, 2015], but the small proportion in Windjana would not be detectable with current technology.

The Windjana sample contains small proportions (near detection limits) of the calcium sulfates anhydrite and bassanite. These phases are likely related to the common veins of Ca sulfate in the Windjana area, like those observed all along Curiosity's path from landing to Kimberley and beyond [e.g., Kronyak *et al.*, 2015; Nachon *et al.*, 2014]. Light-toned veins occur in the Liga, Square Top, and Dillinger members of the Kimberley formation [Grotzinger *et al.*, 2015b] and are observed in the vicinity of Windjana, although no veins are seen within the drill hole.

#### 4.2.4. Diagenetic Feldspar

Diagenetic effects on terrestrial sediments can include replacement/precipitation of significant proportions of alkali feldspars and plagioclase [Fedo *et al.*, 1995; Montanari, 1991; Walker *et al.*, 1978], which are typically ascribed to actions of alkali-rich solutions on preexisting feldspars and clay minerals. Such a diagenetic origin for the feldspars in the Windjana sample seems unlikely for several reasons. The high proportion of feldspars seems inconsistent with a diagenetic origin, although it is possible for low-temperature metasomatism action to produce rocks so rich in alkali feldspar (see below, e.g., Glazner [1988]). The presence of olivine, pyrrhotite, and amorphous materials in the Windjana sample argues against extensive diagenesis and thus formation of so much feldspar by diagenesis.

Below, we consider the possibility that the alkali feldspar in Windjana originated through diagenetic or metasomatic processes not within the Windjana sandstone but in the source area for the sediment.

### 4.3. Provenance of the Windjana Mineral Grains

Among the challenges presented by the Windjana sample is to understand the sources of mineral grains, most importantly its alkali feldspar, and thus its abundant potassium. Felsic rocks on Mars appear to be rare based on orbital spectroscopy, and the few identifications of feldspars made by the Compact Reconnaissance Imaging Spectrometer for Mars are most consistent with anorthositic compositions [Carter and Poulet, 2013; Wray *et al.*, 2013]; to date, no alkali feldspars have been confirmed from orbit. However, alkali-rich igneous rocks have been analyzed in several places in Gale Crater [Sautter *et al.*, 2014, 2015; Schmidt *et al.*, 2014b; Stolper *et al.*, 2013; L. Le Deit *et al.*, submitted manuscript, 2015] and are known from the unique Martian meteorite NWA 7034 (and its pairs) [Agee *et al.*, 2013; Humayun *et al.*, 2013; Santos *et al.*, 2015; Wittmann *et al.*, 2015]. Alkaline igneous rocks are relatively rare on Earth [e.g., Winter, 2010]—primitive alkaline magmas are generally thought to represent low-degree partial melts of fertile, volatile-bearing, peridotite [e.g., Wyllie, 1977; Hirose, 1997; Dasgupta *et al.*, 2007; Gupta, 2015; Stolper *et al.*, 2013] or the partial melting of the residues of such low-degree melts that have crystallized in the lithosphere [e.g., Pilet *et al.*, 2008]. More evolved alkaline magmas (of the types that could crystallize alkali-feldspar) are generally thought to arise via fractional crystallization [Gupta, 2015; Stolper *et al.*, 2013] at intermediate (crustal) pressures

[Nekvasil *et al.*, 2004; Sautter *et al.*, 2015]. Because the Windjana sample is the only potassic alkali-rich rock on Mars to be analyzed for mineralogy (the mugearite rock Jake Matijevic [Sautter *et al.*, 2014; Stolper *et al.*, 2013] was not analyzed by CheMin), it may provide crucial clues to the origins of these rocks in general and to the igneous geology of the Gale Crater region. Here we explore what can be inferred from the Windjana sample alone and later place it into local and regional geological contexts.

Extrapolation from sedimentary rocks to the bedrock that sourced the sediment can be ambiguous, because chemical weathering and physical sorting may have intervened and can cause profound mineralogical and chemical differences between source rock and derived sediment particles. For the Windjana sample, we can infer that there was little effect from chemical weathering or alteration but have little control on determining the effects of physical sorting processes. The Windjana sample likely experienced only limited chemical weathering or alteration because most of its sediment particles are smaller than 100  $\mu\text{m}$  (Figure 3b inset; detection limit with the MAHLI camera) and include easily altered minerals like olivine, sanidine, pyrrhotite, and plagioclase.

It is difficult to know if the Windjana sample is a product of significant mechanical sorting, either hydrologic or eolian. We have little evidence about the source terrains for the sediments, except that they are likely from the northern and northwest rim of Gale Crater. Because the Bradbury Group sediments were transported initially by flowing water, we can assume that some hydraulic sorting occurred by grain size and density [Siebach *et al.*, 2015]. Sediment grains of similar densities and physical properties would not be typically separated hydraulically, i.e., that plagioclase grains would not be sorted from those of sanidine nor augite from pigeonite. However, it is possible that olivine grains could be sorted from pyroxenes, and pyroxenes from feldspars. It is more likely that magnetite would be sorted from all other minerals because of its higher density, but hydraulic sorting would not explain variations in abundance ratios of minerals with similar densities. The Windjana sandstone is interpreted as an eolian reworking and redeposition of these fluvial sediments, which represents an additional physical fractionation process. Even with these complicating factors, mineral abundance ratios and chemical compositions enable several constraints to be placed on the sources of sedimentary particles in the Windjana sandstone.

First, the minerals present in (and absent from) the Windjana sample imply that its sources cannot include most types of metamorphic or hydrothermally altered terrains, either regional or local [McSween *et al.*, 2015; Schwenzer and Kring, 2013]. Windjana consists only of typical igneous minerals and their low-temperature alteration products (see above); it does not contain detectable proportions of minerals that are characteristic of metamorphism or hydrothermal alteration. Nor does it contain minerals that are characteristic of most chemical sediments (e.g., carbonates or silica) except iron formations (e.g., iron oxyhydroxides).

Second, the presence of sanidine indicates that the source of this mineral could not be a plutonic igneous rock or other slowly cooled rock. Under such extended cooling from high temperature, Al and Si in the potassium feldspar would have diffused to form ordered orthoclase or microcline. Potential sources of sanidine include potassic volcanic rocks [Gupta, 2015] and some potassic metasomatic rocks [Glazner, 1988].

Third, the Windjana sample includes sediment from at least two sources, because its abundant sanidine and pigeonite are unlikely to have formed in the same protolith. Nearly all potassic alkaline rocks, such as would contain abundant sanidine, contain only augite pyroxene and not pigeonite [Gupta, 2015; Williams *et al.*, 1982]; exceptions are very rare on Earth (e.g., the Fault Canyon Flow, Arizona [Fuis, 1996]). And potassic metasomatic rocks that contain sanidine either contain no mafic silicates [Fedo *et al.*, 1995; Woodard, 1972], hydrous mafic silicates [Glazner, 1988], or augitic pyroxene [Le Bas, 2008]. The idea that the Windjana sediment is derived from a bedrock source region with more than one igneous rock type, or from multiple source regions with distinct rock types, is not surprising in theory [e.g., Thomas 2011]; but it is gratifying that CheMin data alone allows that inference.

Fourth, the intermediate composition plagioclase and some or all of the mafic phases can be ascribed to subalkaline basaltic protolith(s) or source(s). As discussed above, intermediate to evolved alkaline magma contain augite (and often olivine) phenocrysts [see Wilson, 1989, Table 9.3], and thus augite and olivine in Windjana could have been sourced from alkaline and subalkaline protoliths. Interestingly, Figure 6b shows that the Mg#s of the olivine, augite, and pigeonite in Windjana are consistent with all three phases being in Fe-Mg equilibrium—all three pairs of phases lie on lines in  $\text{Mg}\#^{\text{Phase 1}}$  versus  $\text{Mg}\#^{\text{Phase 2}}$  space defined by coexisting augite-pigeonite, olivine-augite, and olivine-pigeonite from low- to moderate-pressure experiments. This

observation, and the fact that pigeonite is extremely rare in alkaline rocks (as noted above), suggests that all three mafic phases were derived from one or more subalkaline basaltic sources—however, as we discuss below, there is a hint that the abundances of K-feldspar and augite are positively correlated in rocks from the Kimberley area and, finally, it is possible that olivines and pyroxenes sourced from alkaline and subalkaline rocks could, by happenstance, fall on the equilibrium Fe-Mg curves in Figure 6b. If all the mafic phases are from the subalkaline basaltic protolith, and if plagioclase was not sorted from pyroxenes and olivine during sediment transport, this basaltic component contains little plagioclase in relation to its pyroxene—a ratio of ~1:4 compared to a typical Earth or eucrite (asteroidal) basalt with a ratio of ~1:1. Such a plagioclase-poor basaltic rock is comparable to many of the shergottite Martian meteorites [e.g., *McSween and Treiman*, 1998] but is quite distinct from basalts like those at Gusev Crater [*McSween et al.*, 2006] and the basaltic sources of the Rocknest soil drift and the John Klein and Cumberland mudstones [*Blake et al.*, 2013; *Vaniman et al.*, 2014].

Thus, the Windjana sample represents a mixture of sedimentary particles derived from at least three bedrock protoliths. One bedrock source was a potassic trachyte or melatrachyte, which contributed the bulk of the sanidine in the Windjana rock, and possibly some of its augite and olivine. Another bedrock source was a basalt (more like the shergottite Martian meteorites) that contributed pigeonite and plagioclase, and possibly some or all of the olivine and augite. A third source, richer in plagioclase feldspar, is suggested by ChemCam LIBS chemical analyses, as discussed below. The Windjana sample contains excess magnetite compared to likely trachytes or shergottites, and this excess may represent an iron-rich cement.

## 5. Implications for Gale Crater Geology

The Windjana sandstone is among the few samples analyzed by the full suite of instruments on the Curiosity rover and so provides one of the few comprehensive views of the geology and petrology of sediment sources and diagenesis in Gale Crater. Here we consider the Windjana sandstone in the local context of the Kimberley outcrops, within the context of other sedimentary rocks that Curiosity has investigated, and then in the broad context of regional geology around Gale Crater.

### 5.1. Windjana in the Local Context of the Kimberley Area

The Windjana sample is the only one from the Kimberley area that was analyzed by CheMin, so it is crucial to know whether Windjana is typical of a particular geological unit or is somehow unique. To place Windjana into the local geochemical setting, we rely on LIBS chemical analyses by the ChemCam instrument (and their localizations by the rover's imaging systems). The local and regional geological settings of the Kimberley area are summarized in *Grotzinger et al.* [2015b].

The Windjana drill site was chosen as a massive, well-exposed outcrop that satisfied engineering constraints of accessibility and stability for drilling, and not for other chemical or mineralogical reasons—thus, it can be considered as an arbitrary sample of the Dillinger member of the Kimberly formation [*Grotzinger et al.*, 2015b]. The Dillinger member is a flat-lying cross-stratified sandstone unit that rests with geometric discontinuity upon south dipping inclined sandstone beds termed the “cliniform sandstones” [*Grotzinger et al.*, 2015b] of the Square Top member and beneath the massive sandstones of the Mount Remarkable and Beagle members (Figures 1 and 2). In the science campaign at the Kimberley, ChemCam LIBS acquired many analyses of rocks of the Dillinger member and those above and below it, which are discussed in detail by L. Le Deit et al. (submitted manuscript, 2015).

Here we focus on element correlations with potassium because of the abundances of sanidine and  $K_2O$  in the Windjana sample. Figure 7a shows LIBS-analyzed abundances of  $Na_2O$  and  $K_2O$  for rocks in the Kimberley area, designated by rock unit (see also L. Le Deit et al. (submitted manuscript, 2015)). These rocks have higher alkali abundances than most rocks analyzed so far in Gale Crater [*Sautter et al.*, 2014; *Schmidt et al.*, 2014b]. Most of the analysis points from the Dillinger member (including Windjana) show a wide range of  $K_2O$  abundances at relatively constant or slightly increasing  $Na_2O$ , trending up to values of  $K_2O/Na_2O \sim 4$  for the top-most Dillinger and the three spots of the Mount Remarkable member (Figure 7a). Four points in the Dillinger have higher  $Na_2O$  and appear intermediate between the other Dillinger points and those of Square Top and Liga (points Corrara, Wallal, Mondooma, and Yarrada). Samples from the stratigraphically lower Square Top and Liga members are rich in sodium compared to the Dillinger and Mount Remarkable members and have  $K_2O/Na_2O$  near unity (Figure 7a) [*Sautter et al.*, 2014; *Schmidt et al.*, 2014b]. These materials are chemically

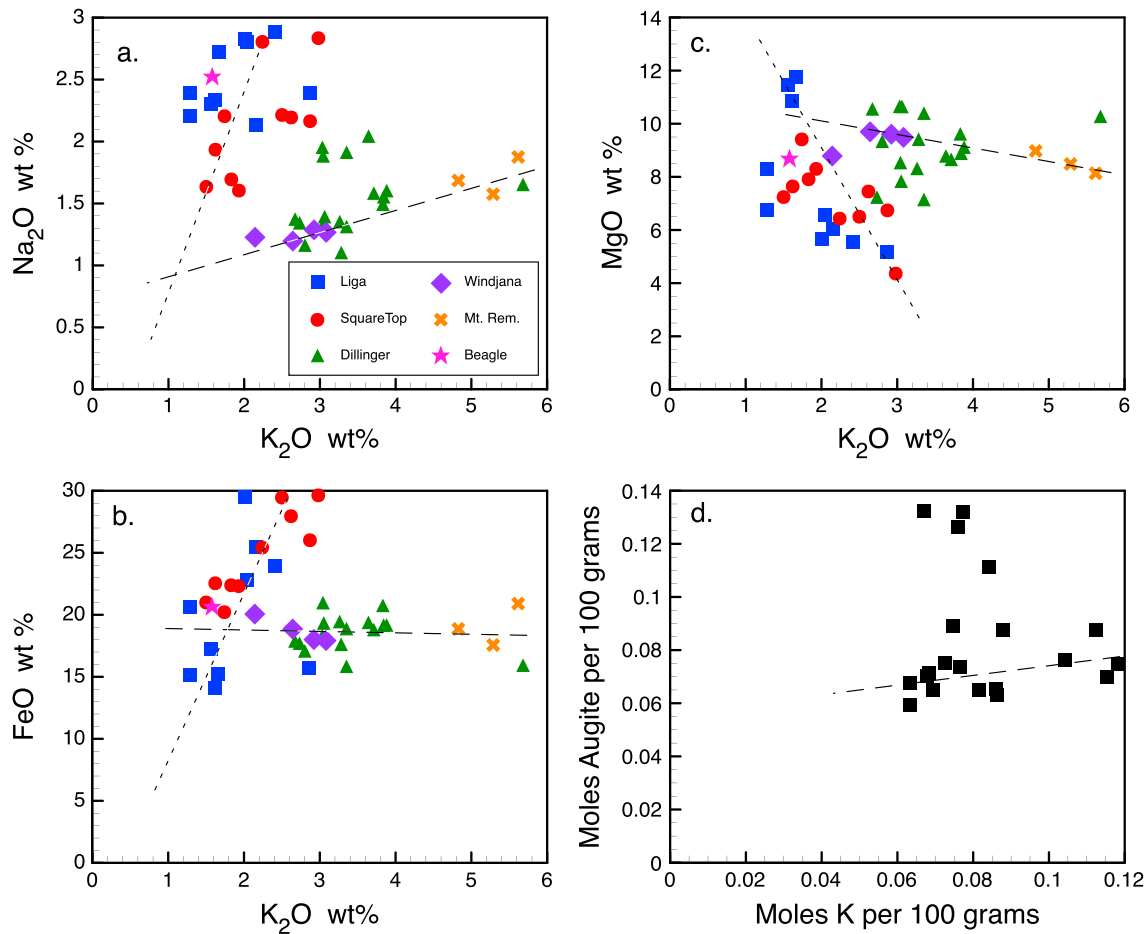


**Figure 7.** Element abundances in rocks of the Kimberley area, from ChemCam analyses (data from NASA PDS). Note that most rocks of the Dillinger member (including Windjana) and the Mount Remarkable member plot near a line on each graph and that most of the other rocks (Liga, Square\_Top, Beagle) fall near a second line. This suggests mixing of three sediment components: one potassic,  $K_2O > 5.6\%$ ,  $FeO(\text{tot}) \approx 18\%$ ,  $MgO < 8\%$ ; one sodic,  $Na_2O > 3\%$ ,  $K_2O > 2.5\%$ ,  $FeO(\text{tot}) > 30\%$ ,  $MgO < 4\%$ ; and one mafic,  $Na_2O \approx 1.5\%$ ;  $K_2O \approx 1.5\%$ ,  $FeO(\text{tot}) \approx 18\%$ ,  $MgO \approx 12\%$ . ChemCam analyses sorted by stratigraphic members: Liga (targets Liga, Yulleroo, Petaluma Elvire, McSherrys, Matheson, Maddox, Harms, Glidden, Nullara); Square\_Top (targets Square\_Top, Square\_Top2, Egan, Elgee, Hooper, Roebuck, TopSquare\_Top, McHale, Esaw); Dillinger (targets Corraa, Forster, Fargoo, Wallal, Jarrad, Cow\_Bore, Kevin's\_Dam, Thangoo, Blinker\_Hill, Paperbark, Pentecost, Mondoomoa, Lodestone, Tumagee, Yarrada, Dillinger); Windjana (targets Windjana\_DRT; minidrill\_tail; maindrill\_tail; hole\_RMI); Mt. Remarkable (targets Mahoney, Mahoney\_2, San\_Sou); and Beagle (target Beagle). (a) Sodium and potassium. Four points from the Dillinger member fall above the general correlation line for Dillinger (and Windjana) and could represent mixtures of the potassic and sodic sediment sources. (b) Iron and potassium abundances. (c) Magnesium and potassium. (d) Molar abundances of K and Ca available to form augite, based on ChemCam analyses [R. Wiens, personal communication]. K is in moles per 100 g of rock, Ca to form augite is moles Ca per 100 g rock, minus the moles Ca required to consume all Al in forming plagioclase:  $Ca_{\text{augite}} = Ca_{\text{tot}} - \frac{1}{2}(Al_{\text{tot}} - Na_{\text{tot}} - K_{\text{tot}})$ . Most data fall on a rough line containing the Windjana analyses and the most K-rich analyses (Dillinger, San\_Sou). The four points with high  $Ca_{\text{augite}}$  and moderate K are the same in Figure 4a that contain Na above its correlation line; this extra Na translates here to higher  $Ca_{\text{augite}}$ .

similar to the Bathurst Inlet rock (analyzed at Yellowknife Bay) [Schmidt *et al.*, 2014a] and related samples [Gellert *et al.*, 2014a, 2014b]. The single analysis of the topmost unit of the Kimberley formation, the Beagle member, is essentially identical in chemical composition to the Square Top member.

The ChemCam LIBS observation points of the Windjana surface material ( $5 \times 5$  raster of the surface) and drill fines are within range of other LIBS observation points in the Dillinger member (Figure 7), and so our inferences above for Windjana mineralogy can be extended to the Dillinger member in general. Also, the spread in  $K_2O$  and  $Na_2O$  abundances for the Dillinger member suggests that it represents mixtures of at least two chemical components (or geochemical processes), in accord with the inferences above from the mineralogy of the Windjana sample. A similar spread of elemental abundances (from ChemCam) data is apparent for  $MgO$  and  $FeO(\text{tot})$ , see Figures 7b and 7c, which allows some additional constraints on the compositions of those components.

From the LIBS analyses, the K-rich component in the Dillinger and Mount Remarkable sandstones is chemically like a potassic trachyte or syenite igneous rock, with  $K_2O \geq 5.5\%$ ,  $K_2O/Na_2O > 3.3$ ,  $FeO$  (tot)  $\approx 18\%$ , and  $MgO < 8\%$  (Figures 7a–7c). This component must be at least as rich in K as the LIBS targets Dillinger (5.7%  $K_2O$ ) and San Sou (5.6%  $K_2O$ ). Thus, its  $K_2O$  content must be  $>1.8$  times that of Windjana and so would contain sanidine in a similar proportion to Windjana, i.e.,  $>40\%$  sanidine. This component could contain significant proportions of mafic minerals (i.e., be a melatrachyte) or could be nearly pure sanidine (i.e., a trachyte).

It is not clear what this trachyte component contains besides sanidine. Abundances of  $FeO$  and  $MgO$  in rocks of the Kimberley (Figures 7b and 7c) are consistent with a relatively low proportions of mafic minerals but could also suggest that all the chemical components contain comparable proportions of mafic minerals. The LIBS analyses are consistent with a positive correlation between molar augite and K (Figure 7d), suggesting that the K-rich component contains  $>1.25$  times as much augite as does Windjana, or  $>27\%$  augite. However, the correlation between molar augite and K is weak (Figure 7d) and could imply nothing. Finally, the mafic silicate minerals in Windjana are consistent with Fe-Mg equilibrium (Figure 6b), which may suggest that they formed in the same igneous protolith and that the trachyte contained only small proportions of mafic silicates [Sautter *et al.*, 2015].

A second chemical component in the Dillinger and Mount Remarkable sandstones can be taken as the lowest- $K_2O$  analyses of that group (Figure 7) or an extrapolation beyond it to lower  $K_2O$ . The extrapolation line (long dashes) crosses a rough line through the Liga, Square Top, and Beagle analyses (short dashes) at  $\sim 1.5\%$   $K_2O$ , and we take that intersection as an approximation of that second chemical component. This second component has a rough average composition of  $K_2O \approx 1.5\%$ ,  $Na_2O \approx 1.5\%$ ,  $FeO$ (tot)  $\approx 18\%$ , and  $MgO \approx 11\%$  (Figures 7a–7c) and approximately half as much augite as Windjana ( $\sim 10\%$  mass, Figure 7d). This component would thus be fairly rich in mafic minerals, likely to be mostly pigeonite and olivine, as its Al abundance would not be consistent with much feldspar. This component could represent material derived from material similar to some shergottite meteorites [e.g., McSween and Treiman, 1998]; chemically, it is similar to average Mars dust [Yen *et al.*, 2005], but the mineralogy of the dust is poorly known.

A third chemical component, apparent in Figure 7, is represented by the most Na-rich analyses of the Liga and Square Top members. This component would have  $Na_2O \geq 3\%$ ,  $K_2O/Na_2O \approx 0.6$ ,  $FeO$ (t)  $\geq 30\%$ , and  $MgO < 4\%$  (Figures 7a–7c). This component is not apparent in the mineralogy or chemistry of the Windjana sample (see above, Figure 7). However, it could be related to dioritic or andesitic igneous rocks encountered elsewhere in Gale Crater [Sautter *et al.*, 2014, 2015] or to some of the sedimentary rocks analyzed southwest of the Kimberley, for instance, the LIBS target Meetinghouse ( $K_2O = 3.8\%$ ,  $Na_2O = 5.2\%$ , and  $K_2O/Na_2O \approx 0.7$ ). For a more comprehensive discussion, see L. Le Deit *et al.* (submitted manuscript, 2015).

These three chemical components cannot be considered exhaustive of all chemical influences on the compositions of sandstones in the Kimberley formation. As shown above, the sediments are cemented by a material consistent with clay + iron oxyhydroxide, which certainly could constitute another chemical component. And an additional chemical component is suggested by the observation that some analyses of the Liga member are close to our hypothesized second component in Mg, Fe, and K (Figures 7b and 7c), while none are close in Na and K (Figure 7a). This discordance suggests that our second component is actually a combination of several components, which might be distinguished in more detailed analysis of the chemical composition data.

## 5.2. Potassic Source Material: Igneous or Metasomatic

It is clear that the Windjana sample is potassic (i.e.,  $K_2O/Na_2O > 1$ ) and that nearby rocks of the Dillinger and Mount Remarkable members are even richer in K and presumably also in alkali feldspar. A simple explanation is that this K-rich contributor to the Windjana sample is sediment from a potassic trachyte lava, an alkaline igneous rock related to others encountered in Gale Crater. However, it is also possible that the potassic component in the Windjana sample is sourced from rocks that experienced K-metasomatic or K-diagenetic processes. At least one rock in Gale Crater (named Preble) shows possible evidence of potassic metasomatism—it includes an area rich in Na, K, and Si that is interpreted as a veinlet rich in alkali feldspar and silica [Sautter *et al.*, 2014]. On Earth, many varieties of metasomatic rock are enriched in potassium and thus alkali feldspar (Table 4), in part because potassium is readily soluble in aqueous and salt-rich fluids, such as those that can form in groundwater or be exsolved from crystallizing magmas [Beratan, 1999; Kodera *et al.*, 2014; Sillitoe, 2010]. The

**Table 4.** Potassic Metasomatic and Diagenetic Alteration: Major Varieties

Name	Association	T (°C)	Alkali Feldspar	Mafic Minerals	References
Fenitization	Alkaline Igneous	~450 to ~700	Microcline, Orthoclase	Pyroxene, mica, amphibole	<i>Le Bas</i> [2008] and <i>Pirajno</i> [2013]
Potassic alteration	Porphyry Copper	~800 to ~450	Microcline, Orthoclase	Biotite, epidote, actinolite	<i>Pirajno</i> [2013] and <i>Sillitoe</i> [2010]
K-metasomatism	Extensional Faulting	<150	Sanidine	Illite, biotite	<i>Beratan</i> [1999] and <i>Glazner</i> [1988]
Diagenesis	Low Temperature	<100	Sanidine	Smectite, glauconite	<i>Fedo et al.</i> [1995], <i>Hay et al.</i> [1988] and <i>Walker et al.</i> [1978]

examples of Table 4 are from the terrestrial experience of rocks enriched in potassium and alkali feldspar, but it is not clear that these rock types (and their parent processes) are possible or present on Mars. However, we cannot discount them in part because evidence for alkaline or potassic igneous rocks on Mars has also been indirect or speculative until recently [*Goodrich et al.*, 2013; *Nekvasil et al.*, 2007; *Santos et al.*, 2015; *Stolper et al.*, 2013]. So we raise the possibility of extensive potassic metasomatism, justified indirectly by evidence and models of extensive hydrothermal alterations around impact craters [*Schwenzer and Kring*, 2013].

Table 4 lists the major types of potassic metasomatism known on Earth (the list is not exhaustive). Potassic metasomatism can occur in wide ranges of geological settings: local authigenesis of sediment; alteration by external formation waters enabled by faults; and magmatohydrothermal alteration around igneous intrusions. However, the potassic sediment component in Windjana, containing sanidine and possibly augite and little if any hydrous silicate minerals, is not obviously consistent with any of these major classes. Near-end-member sanidine can form diagenetically in sediment [*Fedo et al.*, 1995; *Hay et al.*, 1988; *Marshall et al.*, 1986; *Walker et al.*, 1978], in vein deposits [*Cerny and Chapman*, 1986], and in extensive metasomatic bodies associated with major faults [*Beratan*, 1999; *Glazner*, 1988]; in these settings, the characteristic Al-Si disorder of sanidine reflects the random availability of Al and Si in aqueous solutions and not high temperature. However, sanidine in these settings is not accompanied by augitic pyroxene but usually by hydrous mafic minerals [*Fedo et al.*, 1995; *Glazner*, 1988; *Hay et al.*, 1988]. On Earth, diagenesis that yields sanidine alone may be restricted to sediments that lack mafic minerals [e.g., *Marshall et al.*, 1986] and thus are not likely for ancient Mars [*Hay et al.*, 1988; *Marshall et al.*, 1986]. Augitic pyroxene is common in fenites, a style of high-temperature potassic metasomatic rock that develops locally around intrusions of carbonatite and some alkaline igneous magmas. But, befitting their plutonic settings, the alkali feldspar in fenites is microcline or orthoclase [*Castor*, 2008; *Le Bas*, 2008], although there is a report of sanidine in fenite from a carbonatite [*Morogan and Martin*, 1985].

Thus, by elimination, it seems most likely that the potassium-rich sedimentary particles present in the Windjana sample and Dillinger member are erosionally derived from an igneous rock protolith, likely a potassic trachyte. This inference is dictated by the presence of sanidine feldspar and the absence of hydrous silicate minerals. In fact, Curiosity has encountered and investigated several rocks that appear to be trachytes [*Sautter et al.*, 2015]. A problem with identifying the potassic component as igneous trachyte is the composition of the sanidine (~Or<sub>80-100</sub>), which is more potassic (K-rich) than typical for most alkaline volcanic rocks [*Gupta*, 2015]. This would suggest that the trachyte source was ultrapotassic, which is perhaps more characteristic of metasomatic rocks including pseudo-trachytes [*Le Bas*, 2008]. Thus, we cannot exclude a metasomatic source; and it is an interesting possibility that hydrothermal effects around Martian impact craters could include widespread potassic metasomatism [e.g., *Currie*, 1971; *Pesonen et al.*, 2003; *Pirajno*, 2005, 2009; *Vasconcelos et al.*, 2012].

### 5.3. Potassic Igneous Activity

Potassic igneous rocks are rare on Earth, and their genesis is the subject of extensive study and debate [e.g., *Gupta*, 2015]. Silicate melts rich in alkalis can be produced via high-pressure near-solidus melting of volatile-bearing peridotite [e.g., *Dasgupta et al.*, 2007; *Filiberto and Dasgupta*, 2015; *Hirose*, 1997; *Stolper et al.*, 2013; *Treiman and Filiberto*, 2015]. However, generation of potassic and ultrapotassic rocks requires enrichment in K relative to Na. For Mars, K-enrichment cannot be ascribed to planet-wide conditions, as the Mars bulk Na/K ratio is comparable to that of Earth, although abundances of both Na and K are greater than in the Earth [*Dreibus and Wänke*, 1987; *Taylor*, 2013; *Treiman et al.*, 1986]. The Martian meteorite basalts do show a range of Na/K [*Treiman and Filiberto*, 2015], but none of the Martian meteorite basalts are potassic (e.g., K<sub>2</sub>O > Na<sub>2</sub>O).



In the terrestrial mantle, K enrichment (relative to Na) is thought to reflect metasomatic processes involving the localized addition of fluids or very low-degree high-pressure melts to peridotite [e.g., *Foley*, 1992; *Foley et al.*, 2009]. Within the crust, this required that fractionation of K from Na is most commonly ascribed to the action of aqueous fluids or halide melts—Na tends to stay in the silicate melt and crystals (e.g., plagioclase, omphacite pyroxene), while K is preferentially partitioned into the fluids [*Pirajno*, 2013; *Sillitoe*, 2010]. It is not clear whether fluids associated with Martian magmas are water rich or salt rich [*Balta and McSween*, 2013; *Filiberto et al.*, 2014], but the distinction is not crucial here. The important point is that K-rich melts and fluids can be generated (in mantle or crust), move to other sites, and enrich the rocks there in K (e.g., to yield phlogopite-rich peridotite from normal peridotite). Once a K-rich rock has been formed in this way, it can then be melted to yield potassic magmas [*Foley*, 1992].

Evolved alkaline magmas such as trachytes can be generated in several ways and so are not inherently definitive of a geologic or tectonic setting. Trachytic and similar magmas are generally thought to be produced by relatively low-pressure fractional crystallization of alkaline basalts [e.g., *Cousens et al.*, 2003; *Whitaker et al.*, 2007; *Whitaker et al.*, 2008]. Although it has been suggested that trachytic magmas can be produced by direct mantle melting [*Ashwal*, 2015], the ~1 GPa experiments of *Condamine and Médard* [2014] show that the peridotite source must be extremely enriched in K<sub>2</sub>O and that melting must be limited to just above the solidus. Other petrologic processes for generating trachytic magmas include [*Ashwal*, 2015; *Bonin*, 2007; *Condamine and Médard*, 2014; *Gupta*, 2015; *Pilet et al.*, 2008] moderate-volume partial melts of alkali basalts [e.g., *Legendre et al.*, 2005], as products of magma mixing [e.g., *Özdemir et al.*, 2011] and even as partial melts of potassically metasomatized felsic crustal rocks [e.g., *Martin*, 2006] such as those hypothesized in the Gale Crater area [*Sautter et al.*, 2015]. For the Windjana trachytic sediment component, distinguishing among these modes of origin would require data beyond that available: geological and tectonic constraints on the source region and/or trace element and isotopic information.

#### 5.4. Regional Geology of Gale Crater

One of the continuing surprises of the Curiosity MSL mission is the variety of igneous rocks (and igneous-derived sedimentary rocks) in Gale Crater, including alkali-rich types. The first hints of alkali-rich rocks came from ChemCam LIBS chemical analyses at the landing site [*Sautter et al.*, 2014], and were quickly followed by the first APXS analyses of rock samples (Jake Matijevic [*Stolper et al.*, 2013]; Rocknest 3 and Bathurst Inlet [*Schmidt et al.*, 2014b]). By now, there is extensive evidence for a wide range of alkaline igneous rocks (as cobbles in sediments) and sedimentary rocks derived from them [*Sautter et al.*, 2014, 2015; *Schmidt et al.*, 2014b; *Stolper et al.*, 2013; *L. Le Deit et al.*, submitted manuscript, 2015]. The concept that Mars might have produced alkaline magmas is confirmed by the many alkali-rich igneous fragments found in the Martian meteorites NWA 7034 and its pairs [*Humayun et al.*, 2013; *Santos et al.*, 2015; *Wittmann et al.*, 2015] and indirectly confirmed by evidence of alkali affinities of other Martian meteorites [*Goodrich et al.*, 2013; *Nekvasil et al.*, 2007].

However, the igneous protoliths for the Bradbury Group sedimentary rocks (Yellowknife Bay through Kimberley) are very diverse [*Schmidt et al.*, 2014b] and comparable to those of the most diverse volcanic settings on Earth. Ultrapotassic felsic rocks are represented in the Windjana sample (and possibly also in Bathurst Inlet sedimentary rocks [*Blaney et al.*, 2014; *McLennan et al.*, 2014; *Schmidt et al.*, 2014b]); “merely” highly alkaline rocks are represented by the Jake Matijevic rock [*Stolper et al.*, 2013]; “tholeiitic” volcanic rock is the dominant sediment component in the mudstones of Yellowknife Bay [*Vaniman et al.*, 2014]; “shergottitic” basalts (low Al and feldspar) are suggested as contributing to the Windjana sediment; and dioritic/andesitic rocks are known from ChemCam LIBS analyses of rock fragments along Curiosity’s traverse [*Sautter et al.*, 2014; *Sautter et al.*, 2015]. These rocks and sediments were transported into Gale Crater from its northern rim [*Grotzinger et al.*, 2015b], which therefore must include an extensive array of igneous rocks.

The range of igneous composition seen so far in Gale Crater can be appreciated on a TAS (total alkalis versus silica) diagram, Figure 8, which is a standard presentation for classification of Earth’s igneous rocks [*Le Maitre et al.*, 2002]. On Figure 8 are plotted LIBS chemical analyses of the recognized igneous rocks encountered by Curiosity [*Sautter et al.*, 2015] and the composition of the Dillinger sandstone (K<sub>2</sub>O/Na<sub>2</sub>O ratios given on the graph). Lava compositions from the St. Helena ocean island volcano are shown for comparison [*Kawabata et al.*, 2011]. On the TAS diagram, lavas of other ocean island volcanoes show trajectories like that of the St. Helena lavas but at different total alkalis for a given silica content or with different K<sub>2</sub>O/Na<sub>2</sub>O ratios. For

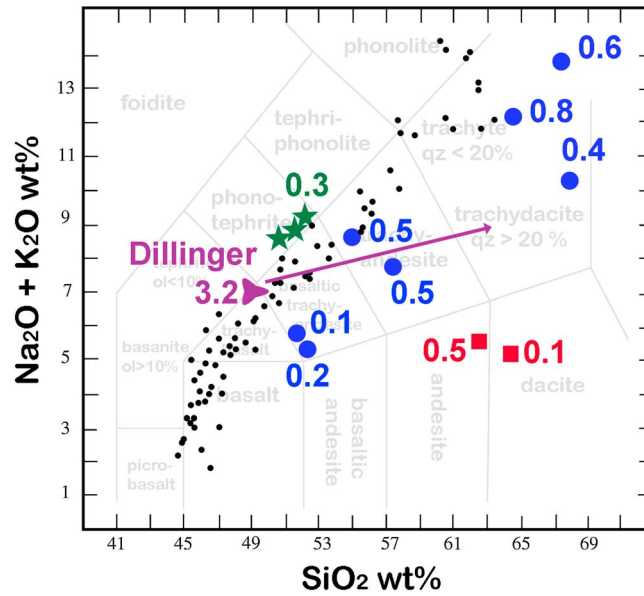


**Figure 8.** TAS diagram (total alkalis-silica) diagram of igneous rock classification [Le Maitre et al., 2002], showing the Dillinger sample in relation to other igneous rocks of Earth and Gale Crater. The K-rich sediment component in the Windjana sample, here represented by an average of ChemCam LIBS analyses of the Dillinger and Mount Remarkable members, is the purple trillium; subtraction of Fe-O-(H) cement from the analysis (see text) would move the composition along the purple arrow toward a trachyte composition. Other igneous rocks identified and analyzed by LIBS include “dioritic” samples in red squares and alkaline rocks in blue circles [Sautter et al., 2015]. The Jake Matijevec rock, a mugearite, is shown as green stars [Stolper et al., 2013]. For comparison, the black dots show lava compositions from the ocean island of St. Helena [Kawabata et al., 2011], a typical igneous trend consistent with fractionation of olivine ( $\text{SiO}_2 \sim 40\%$ ,  $\text{K}_2\text{O} + \text{Na}_2\text{O} = 0$ ). The number near each symbol (same color as the symbol) is  $\text{K}_2\text{O}/\text{Na}_2\text{O}$  for that analysis; the Gale Crater igneous samples span a wide range of  $\text{K}_2\text{O}/\text{Na}_2\text{O}$ , with the Dillinger analysis being the highest of all. For comparison, all of the St. Helena samples (despite their range in  $\text{SiO}_2$  contents) have  $\text{K}_2\text{O}/\text{Na}_2\text{O}$  near 2.5.

source (mantle) material at different pressures [Collinet et al., 2015; Whitaker et al., 2007], but trends of different  $\text{K}_2\text{O}/\text{Na}_2\text{O}$  must represent different source materials or chemical processes (e.g., metasomatism).

### 5.5. Comparison to Ancient Earth

The northern rim of Gale Crater exposes rocks of an extremely varied igneous province of Noachian age [Farley et al., 2014; Le Deit et al., 2013; Thomson et al., 2011], which includes several sorts of basalts (tholeiitic, “shergottitic,” alkaline), evolved igneous rocks (dioritic, syenitic, potassic), and possibly anorthosite [Sautter et al., 2014]. This igneous variety is significantly greater than that of the few known Earth rocks and mineral grains of comparable age (~4.2 Ga) and is possibly comparable in variety only to Earth rocks younger than ~2.7 Ga (near the Archean-Proterozoic transition), [see Blichert-Toft et al., 1996; Nisbet, 1987; Taylor and McLennan, 2009].

The Earth’s surface at ~4.2 Ga, when the rocks of the Gale Crater rim formed [Farley et al., 2014], is poorly known but appears to have been significantly different and less complex than at Gale. Available data suggest that it was similar to that of later, mid-Achaean times: continental masses dominated by the TTG rock association (tonalite, trondhjemite, granodiorite); ocean basins dominated by MORB-like basalts and komatiites, and ubiquitous water [Valley et al., 2002]. Perhaps the only preserved rock mass from this time is the Nuvvanada [O’Neil et al., 2008, 2012]. Its rocks are typical of common Archean greenstone belts and consisted (before metamorphism) of basaltic to picritic igneous rocks with interbeds of banded iron formation [O’Neil et al., 2007], which can be interpreted as ocean basin basalts and chemical sediments (comparable

example, lavas of Flores volcano (Azores Islands) fall along nearly the same TAS trajectory as the St. Helena lavas, but have  $\text{K}_2\text{O}/\text{Na}_2\text{O}$  of ~0.3 [Genske et al., 2012], compared to St. Helena’s  $\text{K}_2\text{O}/\text{Na}_2\text{O}$  of ~2.5 [Kawabata et al., 2011].

From Figure 8, it is clear that the Gale Crater igneous rocks fall on several distinct TAS trajectories, as shown by Sautter et al. [2015]. The few dioritic samples (red on Figure 8) are subalkaline and could conceivably be related to the source of basaltic sediments of the Cumberland and John Klein samples [Vaniman et al., 2014]. The mildly alkaline igneous rocks (blue on Figure 8) are consistent with an igneous trend parallel to that of the St. Helena lavas, but likely represent two distinct fractionation series with different  $\text{K}_2\text{O}/\text{Na}_2\text{O}$  ratios (~0.1 and ~0.5). The strongly alkaline Jake Matejvic rock is unique and not related to the other igneous rocks. And the potassic component of the Dillinger (and Windjana) samples cannot be closely related to any of the other Gale igneous rocks because of its extreme  $\text{K}_2\text{O}/\text{Na}_2\text{O}$  value of 3.2 (Figure 8). It is reasonable that the trends with similar  $\text{K}_2\text{O}/\text{Na}_2\text{O}$  could represent fractionations of the same

to the modern “Steinman trinity” rocks of ophiolites). Evidence for continent-like crust at ~4.2 Ga comes primarily from zircon grains in younger sandstone, notably the Jack Hills of Australia [Harrison, 2009]. Many of these ancient zircon grains contain inclusions of quartz and feldspars, linking them to felsic igneous rocks. Many of the zircon grains have heavy oxygen ( $\delta^{18}\text{O}$  values), which implies that their parent magmas interacted with low-temperature water [Harrison, 2009; Valley et al., 2002], i.e., oceans. Some of the zircons contain inclusions of muscovite mica, implying the presence of S-type granitic rocks, which are inferred to form by melting of clay-bearing (i.e., aqueously weathered) sediments [Hopkins et al., 2008]. In the Gale Crater sediments, we see evidence for all of these terrestrial materials (basalts, picrite, granodiorite, and aqueously altered sediments), although not micas nor S-type granitic rocks.

However, the sediments of Gale Crater include rocks and chemical components implying that their source regions contained alkaline igneous rocks, which are not known in the terrestrial rock record in rocks older than ~2.7 Ga [Blichert-Toft et al., 1996; Kogarko, 2006]. At that time, near the transition from Archean to Proterozoic epochs, alkaline igneous rocks appear in varied tectonic settings across the globe: the Abitibi and Wawa greenstone belts of Canada [Kitayama and Francis, 2014; Sutcliffe et al., 1990], the Yilgarn of Australia [Smithies and Champion, 1999]; the Kola peninsula of Russia [Zozulya et al., 2005], and the Asward complex of Morocco [Bea et al., 2014]. Interestingly, the Wawa alkaline rocks (emplaced ~2.7 Ga) include ferropicrites [Kitayama and Francis, 2014], similar to magma types inferred in the petrogenesis of Martian basaltic and picritic meteorites [Filliberto et al., 2008].

So in very broad terms, the igneous rocks exposed in the vicinity of Gale Crater (at least as known from sediments shed from them into the Crater), are more complex and varied than those of comparable-aged rocks on Earth. If comparison can be made, the Gale Crater igneous rocks are more comparable than to latest Archean and early Proterozoic rocks on Earth, at least in terms of the presence of alkaline igneous rocks. The reasons behind the absence of alkaline rocks in the pre-2.7 Ga Earth are not clear [Blichert-Toft et al., 1996; Kogarko, 2006]. A possible explanation for both Earth and Mars is that alkaline rocks (and their precursor mantle metasomatic effects) require low-volume partial melts and thus cannot form in hot mantles where high-volume partial melts are the norm [Blichert-Toft et al., 1996; Herzberg et al., 2010]. In this scenario, Mars would have cooled down to the point of allowing low-volume partial melts before 4.2 Ga, while the Earth only cooled this far at ~2.7 Ga. This analogy is in accord with thermochemical modeling of the Martian mantle, in which mantle potential temperatures in Mars’ Noachian time (including 4.2 Ga) are calculated to be several hundred degrees lower than the Earth’s at a comparable time [Baratoux et al., 2013; Filliberto and Dasgupta, 2015].

#### Acknowledgments

The authors are grateful to the whole MSL Curiosity team, both engineers and scientists, who have made the mission possible and these data available. We are particularly grateful to the engineers who designed and built CheMin, the drill system (SA/SpAH), and the CHIMRA sieve/delivery system. Primary data used here are publically available through the NASA Planetary Data System (<https://pds.nasa.gov>); additional data are in the supporting information and from the authors. We are grateful to S. Potter-McIntyre, D. Baratoux (Associate Editor), and two anonymous reviewers for insightful and helpful critiques. NASA funded this research via contracts with the Jet Propulsion Laboratory, California Institute of Technology; part of this research was carried out at the Jet Propulsion Laboratory, California Institute of Technology, under a contract with the National Aeronautics and Space Administration. Naming of commercial products or software packages is for documentation, and does not constitute endorsement by NASA, JPL, or the authors. LPI Contribution 1888.

## 6. Conclusion

These mineralogical and chemical interpretations of the Windjana sample, in its geological context, provide intriguing but understandably incomplete glimpses into the history of Gale Crater and Mars. The Windjana sample is characteristic of its source unit, the Dillinger, which is interpreted as an eolian sand unit among fluvial deposits [Grotzinger et al., 2015b]. But the Dillinger is significantly richer in potassium (and presumably in sanidine) from those of the units around it, implying that the Dillinger is not merely a local reworking of the underlying sandstones. The sources of the sediment in the Windjana sample is not known, but is likely to be mostly from the northern rim of Gale Crater; and it is likely that the sand was transported primarily by flowing water and then remobilized and redeposited by wind [Grotzinger et al., 2015b]. It remains unclear how the sediment was generated from the protolith—how did nature conspire to form and transport silt- and mud-sized grains without evidence of aqueous alteration of their olivine and sanidine? The source lithologies for the Windjana sample’s sediments represent a complex igneous province, which includes (at least) potassic trachyte, plagioclase-rich basalt (i.e., tholeiitic), and mafic basalt (i.e., shergottitic). Together, these imply the actions of complex igneous processes (crustal and mantle) in Mars’ Noachian or early Hesperian epochs, and (presuming that Gale Crater is not a unique locale) that Mars’ ancient highlands should present a significant diversity of rock types [Santos et al., 2015; Sautter et al., 2015].

## References

- Agee, C. B., et al. (2013), Unique meteorite from early Amazonian Mars: Water-rich basaltic breccia Northwest Africa 7034, *Science*, 339, 780–783.
- Allan, J. E. M., J. M. D. Coey, I. S. Sanders, U. Schwertmann, G. Friedrich, and A. Wiechowski (1989), An occurrence of a fully-oxidized natural titanomaghemite in basalt, *Mineral. Mag.*, 53(371), 299–304.

- Anderson, R. B., and J. F. I. Bell (2010), Geologic mapping and characterization of Gale Crater and implications for its potential as a Mars Science Laboratory landing site, *Int. J. Mars Sci. Explor.*, *5*, 76–128.
- Anderson, R. C., et al. (2012), Collecting samples in Gale crater, Mars; an overview of the Mars Science Laboratory Sample Acquisition, Sample Processing and Handling System, *Space Sci. Rev.*, *170*, 57–75.
- Anderson, R. C., et al. (2015a), The Mars Science Laboratory scooping campaign at Rocknest, *Icarus*, *256*, 66–77.
- Anderson, R. C., J. Bridges, A. Williams, L. Edgar, A. Ollila, J. Williams, M. Nachon, N. Mangold, M. Fisk, and J. Schieber (2015b), ChemCam results from the Shaler outcrop in Gale crater, Mars, *Icarus*, *249*, 2–21.
- Antao, S. M., I. Hassan, and J. B. Parise (2005), Cation ordering in magnesioferrite,  $MgFe_2O_4$ , to 982 C using in situ synchrotron X-ray powder diffraction, *Am. Mineral.*, *90*, 219–228.
- Ashwal, L. D. (2015), Trachyte petrogenesis, Abstract 3126 presented at Goldschmidt Conference 2015.
- Bailey, S. W. (1988), Chlorites: Structures and crystal chemistry, in *Hydrous Phyllosilicates (Exclusive of Micas)*, edited by S. W. Bailey, pp. 347–404, Mineral. Soc. of Am., Washington, D. C.
- Balta, J. B., and H. Y. McSween (2013), Water and the composition of Martian magmas, *Geology*, *41*(10), 1115–1118.
- Baratoux, D., M. Toplis, M. Monnereau, and V. Sautter (2013), The petrological expression of early Mars volcanism, *J. Geophys. Res. Planets*, *118*, 59–64, doi:10.1029/2012JE004234.
- Barnes, S. J., and P. L. Roeder (2001), The range of spinel compositions in terrestrial mafic and ultramafic rocks, *J. Petrol.*, *42*(12), 2279–2302.
- Bea, F., P. Montero, F. Haissen, E. Rjimiati, J. Molina, and J. Scarrow (2014), Kalsilite-bearing plutonic rocks: The deep-seated Archean Awasir massif of the Reguibat Rise, South Morocco, West African Craton, *Earth Sci. Rev.*, *138*, 1–24.
- Beratan, K. K. (1999), Miocene potassium metasomatism, Whipple Mountains, southeastern California: A datable tracer of extension-related fluid transport, *Geology*, *27*, 259–262.
- Bibi, I., B. Singh, and E. Silvester (2011), Akaganéite ( $\beta$ -FeOOH) precipitation in inland acid sulfate soils of south-western New South Wales (NSW), Australia, *Geochim. Cosmochim. Acta*, *75*, 6429–6438.
- Bish, D. L., et al. (2013), X-ray diffraction results from Mars Science Laboratory: Mineralogy of Rocknest at Gale Crater, *Science*, *341*(6153), doi:10.1126/science.1238932.
- Bishop, J. L., E. Murad, and M. D. Dyar (2015), Akaganéite and schwertmannite: Spectral properties and geochemical implications of their possible presence on Mars, *Am. Mineral.*, *100*(4), 738–746.
- Blake, D. F., et al. (2012), Characterization and calibration of the CheMin mineralogical instrument on Mars Science Laboratory, *Space Sci. Rev.*, *170*(1–4), 341–399.
- Blake, D. F., et al. (2013), Curiosity at Gale Crater, Mars: Characterization and analysis of the Rocknest sand shadow, *Science*, *341*(6153), doi:10.1126/science.1239505.
- Blaney, D., R. Wiens, S. Maurice, S. Clegg, R. Anderson, L. Kah, S. Le Mouelic, A. Ollila, N. Bridges, and R. Tokar (2014), Chemistry and texture of the rocks at Rocknest, Gale Crater: Evidence for sedimentary origin and diagenetic alteration, *J. Geophys. Res. Planets*, *119*, 2109–2131, doi:10.1002/2013JE004590.
- Blasi, A. (1977), Calculation of T-site occupancies in alkali feldspar from refined lattice constants, *Mineral. Mag.*, *41*, 525–526.
- Blichert-Toft, J., N. Arndt, and J. Ludden (1996), Precambrian alkaline magmatism, *Lithos*, *37*(2), 97–111.
- Bonin, B. (2007), A-type granites and related rocks: Evolution of a concept, problems and prospects, *Lithos*, *97*(1), 1–29.
- Bosi, F., U. Hälenius, and H. Skogby (2009), Crystal chemistry of the magnetite-ulvöspinel series, *Am. Mineral.*, *94*, 181–189.
- Bristow, T. F., et al. (2015), The origin and implications of clay minerals from Yellowknife Bay, Gale Crater, Mars, *Am. Mineral.*, *100*, 824–836, doi:10.2138/am-2015-5077CCBYNCND.
- Cai, J., J. Liu, Z. Gao, A. Navrotsky, and S. L. Suib (2001), Synthesis and anion exchange of tunnel structure akaganéite, *Chem. Mater.*, *13*, 4595–4602.
- Campbell, J. L., G. M. Perrett, R. Gellert, S. M. Andrushenko, N. I. Boyd, J. A. Maxwell, P. L. King, and C. D. Schofield (2012), Calibration of the Mars Science Laboratory alpha particle X-ray spectrometer, *Space Sci. Rev.*, *170*(1–4), 319–340.
- Carter, J., and F. Poulet (2013), Ancient plutonic processes on Mars inferred from the detection of possible anorthositic terrains, *Nat. Geosci.*, *6*(12), 1008–1012.
- Carter, J., C. Viviano-Beck, D. Loizeau, J. Bishop, and L. Le Deit (2015), Orbital detection and implications of akaganéite on Mars, *Icarus*, *253*, 296–310.
- Castor, S. B. (2008), The Mountain Pass rare-earth carbonatite and associated ultrapotassic rocks, California, *Can. Mineral.*, *46*, 779–806.
- Cerny, P., and R. Chapman (1986), Adularia from hydrothermal vein deposits: Extremes in structural state, *Can. Mineral.*, *24*, 717–728.
- Chichagov, A. V., D. A. Varlamov, R. A. Dilanyan, T. N. Dokina, N. A. Drozhzhina, O. L. Samokhvalova, and T. V. Ushakovskaya (2001), MINCRYST: A crystallographic database for minerals, local and network (WWW) versions, *Crystallogr. Rep.*, *46*(5), 876–879.
- Chiper, S. J., and D. L. Bish (2002), FULLPAT: A full-pattern quantitative analysis program for X-ray powder diffraction using measured and calculated patterns, *J. Appl. Crystallogr.*, *35*(6), 744–749.
- Chiper, S. J., and D. T. Vaniman (2007), Experimental stability of magnesium sulfates hydrates that may be present on Mars, *Geochim. Cosmochim. Acta*, *71*, 241–250.
- Collinet, M., E. Médard, B. Charlier, J. Vander Auwera, and T. L. Grove (2015), Melting of the primitive Martian mantle at 0.5–2.2 GPa and the origin of basalts and alkaline rocks on Mars, *Earth Planet. Sci. Lett.*, *427*, 83–94.
- Collyer, S., N. W. Grimes, D. J. Vaughan, and G. Longworth (1988), Studies of the crystal structure and crystal chemistry of titanomaghemite, *Am. Mineral.*, *73*, 153–160.
- Condamine, P., and E. Médard (2014), Experimental melting of phlogopite-bearing mantle at 1 GPa: Implications for potassic magmatism, *Earth Planet. Sci. Lett.*, *397*, 80–92.
- Cousens, B. L., D. A. Clague, and W. D. Sharp (2003), Chronology, chemistry, and origin of trachytes from Hualalai Volcano, Hawaii, *Geochem. Geophys. Geosyst.*, *4*(9), 1078, doi:10.1029/2003GC000560.
- Critelli, S., and R. V. Ingersoll (1995), Interpretation of neovolcanic versus palaeovolcanic sand grains: An example from Miocene deep-marine sandstone of the Topanga Group (Southern California), *Sedimentology*, *42*, 783–804.
- Currie, K. (1971), A study of potash fertilization around the Brent crater, Ontario—A paleozoic alkaline complex, *Can. J. Earth Sci.*, *8*(5), 481–497.
- Dasgupta, R., M. M. Hirschmann, and N. D. Smith (2007), Partial melting experiments of peridotite +  $CO_2$  at 3 GPa and genesis of alkalic ocean island basalts, *J. Petrol.*, *48*(11), 2093–2124.
- Dehouck, E., S. M. McLennan, P.-Y. Meslin, and A. Cousin (2014), Constraints on abundance, composition, and nature of X-ray amorphous components of soils and rocks at Gale crater, Mars, *J. Geophys. Res. Planets*, *119*, 1–18, doi:10.1002/2014JE004716.
- Dera, P., K. Zhuravlev, V. Prakapenka, M. L. Rivers, J. Finkelstein, O. Rubor-Urošević, O. Tschauer, S. M. Clark, and R. T. Downs (2013), High pressure single-crystal micro X-ray diffraction analysis with GSE\_ADA/RSV software, *High Pressure Res.*, *33*(3), 466–484.

- Dreibus, G., and H. Wänke (1987), Volatiles on Earth and Mars: A comparison, *Icarus*, *71*(2), 225–240.
- Edgar, L., D. Rubin, J. Schieber, S. Gupta, R. Williams, K. Stack, M. Rice, J. Grotzinger, K. Lewis, and M. Malin (2014), Reconstructing ancient fluvial environments at the Balmville and Dingo Gap outcrops, Gale crater, Mars, Abstract P42C-05 presented at AGU Fall Meeting, San Francisco, Calif.
- Farley, K., C. Malespin, P. Mahaffy, J. Grotzinger, P. Vasconcelos, R. Milliken, M. Malin, K. Edgett, A. Pavlov, and J. Hurowitz (2014), In situ radiometric and exposure age dating of the Martian surface, *Science*, *343*(6169), doi:10.1126/science.1247166.
- Farrand, W. H., T. D. Glotch, and B. Horgan (2014), Detection of copiapite in the northern Mawrth Vallis region of Mars: Evidence of acid sulfate alteration, *Icarus*, *241*, 346–357.
- Fedo, C. M., H. W. Nesbitt, and G. M. Young (1995), Unraveling the effects of potassium metasomatism in sedimentary rocks and paleosols, with implications for paleoweathering conditions and provenance, *Geology*, *23*(10), 921–924.
- Filiberto, J., and R. Dasgupta (2011), Fe<sup>2+</sup>-Mg partitioning between olivine and basaltic melts: Applications to genesis of olivine-phyric shergottites and conditions of melting in the Martian interior, *Earth Planet. Sci. Lett.*, *304*, 527–537.
- Filiberto, J., and R. Dasgupta (2015), Constraints on the depth and thermal vigor of melting in the Martian mantle, *J. Geophys. Res. Planets*, *120*, 109–122, doi:10.1002/2014JE004745.
- Filiberto, J., A. H. Treiman, and L. Le (2008), Crystallization experiments on a Gusev Adirondack basalt composition, *Meteorit. Planet. Sci.*, *43*(7), 1137–1146.
- Filiberto, J., A. H. Treiman, P. A. Giesting, C. A. Goodrich, and J. Gross (2014), High-temperature chlorine-rich fluid in the Martian crust: A precursor to habitability, *Earth Planet. Sci. Lett.*, *401*, 110–115.
- Foley, S. F. (1992), Vein-plus-wall-rock melting mechanisms in the lithosphere and the origin of potassic alkaline magmas, *Lithos*, *28*(3), 435–453.
- Foley, S. F., G. M. Yaxley, A. Rosenthal, S. Buhre, E. S. Kiseeva, R. P. Rapp, and D. E. Jacob (2009), The composition of near-solidus melts of peridotite in the presence of CO<sub>2</sub> and H<sub>2</sub>O between 40 and 60 kbar, *Lithos*, *112*, 274–283.
- Forni, O., D. Vaniman, L. Le Deit, S. Clegg, N. Lanza, J. Lasue, D. Bish, N. Mangold, R. Wiens, and P.-Y. Meslin (2015), Fluorine and lithium at the Kimberley outcrop, Gale Crater, presented at Abstract 1989 Lunar and Planetary Science Conference, 46.
- Freeze, R. A., and J. A. Cherry (1979), *Groundwater*, 604 pp., Prentice-Hall, Englewood Cliffs, N. J.
- Fuis, G. S. (1996), *The Geology and Mechanics of Formation of the Fort Rock Dome, Yavapai County, Arizona*, U.S. Geol. Surv. Prof. Pap., vol. 1266, pp. 1–95, U.S. Gov. Print. Off., Washington, D. C.
- Garrels, R. M., and C. L. Christ (1990), *Solutions, Minerals, and Equilibria*, 2nd ed., 450 pp., Jones and Bartlett, Boston, Mass.
- Gattacceca, J., P. Rochette, R. Scorzelli, P. Munayco, C. Agee, Y. Quesnel, C. Courmède, and J. Geissman (2014), Martian meteorites and Martian magnetic anomalies: A new perspective from NWA 7034, *Geophys. Res. Lett.*, *41*, 4859–4864, doi:10.1002/2014GL060464.
- Gellert, R., J. Berger, N. Boyd, J. Campbell, B. Elliott, A. Fairen, P. King, L. Leshin, B. Pavri, and G. Perrett (2014a), APXS measurements along the MSL traverse at Gale Crater, Mars, *LPI Contrib.*, *1791*, 1327.
- Gellert, R., et al. (2014b), APXS Chemical Composition of the Kimberley Sandstone in Gale Crater, Abstract P34A-05 presented at 2014 Fall Meeting, AGU, San Francisco, Calif.
- Genske, F. S., S. P. Turner, C. Beier, and B. F. Schaefer (2012), The petrology and geochemistry of lavas from the western Azores islands of Flores and Corvo, *J. Petrol.*, *53*(8), 1673–1708.
- Glazner, A. F. (1988), Stratigraphy, structure, and potassic alteration of Miocene volcanic rocks in the Sleeping Beauty area, central Mojave Desert, California, *Geol. Soc. Am. Bull.*, *100*, 424–435.
- Golla-Schindler, U., H. S. C. O'Neill, and A. Putnis (2005), Direct observation of spinodal decomposition in the magnetite-hercynite system by susceptibility measurements and transmission electron microscopy, *Am. Mineral.*, *90*, 1278–1283.
- Goodrich, C. A., A. H. Treiman, J. Filiberto, J. Gross, and M. Jercinovic (2013), K<sub>2</sub>O-rich trapped melt in olivine in the Nakhla meteorite: Implications for petrogenesis of nakhlites and evolution of the Martian mantle, *Meteorit. Planet. Sci.*, *48*(12), 2371–2405.
- Gorski, C. A., and M. M. Scherer (2010), Determination of nanoparticulate magnetite stoichiometry by Mössbauer spectroscopy, acidic dissolution, and powder X-ray diffraction: A critical review, *Am. Mineral.*, *95*, 1017–1026.
- Grotzinger, J. P., J. Crisp, A. R. Vasavada, R. C. Anderson, C. J. Baker, R. Barry, D. F. Blake, P. Conrad, K. S. Edgett, and B. Ferdowski (2012), Mars Science Laboratory mission and science investigation, *Space Sci. Rev.*, *170*(1–4), 5–56.
- Grotzinger, J. P., D. Sumner, L. Kah, K. Stack, S. Gupta, L. Edgar, D. Rubin, K. Lewis, J. Schieber, and N. Mangold (2014), A habitable fluvio-lacustrine environment at Yellowknife Bay, Gale Crater, Mars, *Science*, *343*(6169), 1,242,777.
- Grotzinger, J. P., J. A. Crisp, and A. R. Vasavada (2015a), Curiosity's mission of exploration at Gale Crater, Mars, *Elements*, *11*(1), 19–26.
- Grotzinger, J. P., et al. (2015b), Deposition, exhumation, and paleoclimate of an ancient lake deposit, Gale Crater, Mars, *Science*, *350*(6257), doi:10.1126/science.aac7575.
- Gupta, A. K. (2015), *Origin of Potassium-Rich Silica-Deficient Igneous Rocks*, 536 pp., Springer, New York, doi:10.1007/978-81-322-2083-1.
- Hamecher, E. A., P. M. Antonshchikina, M. A. Ghiorso, and P. D. Azimow (2013), The molar volume of FeO-MgO-Fe<sub>2</sub>O<sub>3</sub>-Cr<sub>2</sub>O<sub>3</sub>-Al<sub>2</sub>O<sub>3</sub>-TiO<sub>2</sub> spinels, *Contrib. Mineral. Petrol.*, *165*(1), 25–43.
- Harries, D., K. Pollok, and F. Langenhorst (2013), Oxidative dissolution of 4C- and NC-pyrrhotite: Intrinsic reactivity differences, pH dependence, and the effect of anisotropy, *Geochim. Cosmochim. Acta*, *102*, 23–44.
- Harrison, T. M. (2009), The Hadean crust: Evidence from > 4 Ga zircons, *Annu. Rev. Earth Planet. Sci.*, *37*, 479–505.
- Hay, R. L., M. Lee, D. R. Kolata, J. C. Matthews, and J. C. Morton (1988), Episodic potassic diagenesis of Ordovician tuffs in the Mississippi Valley area, *Geology*, *16*, 743–747.
- Herzberg, C., K. Condie, and J. Korenaga (2010), Thermal history of the Earth and its petrological expression, *Earth Planet. Sci. Lett.*, *292*(1), 79–88.
- Hirose, K. (1997), Partial melt compositions of carbonated peridotite at 3 GPa and role of CO<sub>2</sub> in alkali-basalt magma generation, *Geophys. Res. Lett.*, *24*(22), 2837–2840, doi:10.1029/97GL02956.
- Holm, N. G., M. J. Dowler, T. Wadsten, and G. Arrhenius (1983), β-FeOOH · Cl<sub>n</sub> (akaganéite) and Fe<sub>1-x</sub>O (wüstite) in hot brine from the Atlantis II Deep (Red Sea) and the uptake of amino acids by synthetic β-FeOOH · Cl<sub>n</sub>, *Geochim. Cosmochim. Acta*, *47*, 1465–1470.
- Hopkins, M., T. M. Harrison, and C. E. Manning (2008), Low heat flow inferred from > 4 Gyr zircons suggests Hadean plate boundary interactions, *Nature*, *456*(7221), 493–496.
- Humayun, M., A. Nemchin, B. Zanda, R. Hewins, M. Grange, A. Kennedy, J.-P. Lorand, C. Göpel, C. Fieni, and S. Pont (2013), Origin and age of the earliest Martian crust from meteorite NWA 7533, *Nature*, *503*(7477), 513–516.
- Johnson, J. R., J. F. Bell, S. Bender, D. Blaney, E. Cloutis, L. DeFlores, B. Ehlmann, O. Gasnault, B. Gondet, and K. Kinch (2015a), ChemCam passive reflectance spectroscopy of surface materials at the Curiosity landing site, Mars, *Icarus*, *249*, 74–92.
- Johnson, J. R., R. C. Wiens, S. Maurice, D. Blaney, O. Gasnault, E. Cloutis, S. LeMouelic, and S. Bender (2015b), ChemCam passive reflectance spectroscopy of ferric sulfates and ferric oxides near the base of Mt. Sharp, Abstract 1433 presented at 46th Lunar and Planet. Sci. Conf.

- Kawabata, H., T. Hanyu, Q. Chang, J.-I. Kimura, A. R. Nichols, and Y. Tatsumi (2011), The petrology and geochemistry of St. Helena alkali basalts: Evaluation of the oceanic crust-recycling model for HIMU OIB, *J. Petrol.*, *52*(4), 791–838.
- Kitayama, Y. C., and D. Francis (2014), Iron-rich alkaline magmatism in the Archean Wawa greenstone belts (Ontario, Canada), *Precambrian Res.*, *252*, 53–70.
- Kodera, P., C. A. Heinrich, M. Wälle, and J. Lexa (2014), Magmatic salt melt and vapor: Extreme fluids forming porphyry gold deposits in shallow subvolcanic settings, *Geology*, *42*(6), 495–498.
- Kogarko, L. (2006), Alkaline magmatism and enriched mantle reservoirs: Mechanisms, time, and depth of formation, *Geochem. Int.*, *44*(1), 3–10.
- Kroll, H., and P. H. Ribbe (1983), Lattice parameters, composition, and Al-Si order in alkali feldspars, in *Feldspar Mineralogy*, 2nd ed., edited by P. H. Ribbe, pp. 57–99, Mineral. Soc. of Am., Washington, D. C.
- Kroll, H., and P. H. Ribbe (1987), Determining (Al,Si) distribution and strain in alkali feldspars using lattice parameters and diffraction peak positions: A review, *Am. Mineral.*, *72*, 491–506.
- Kronyak, R. E., L. C. Kah, M. Nachon, N. Mangold, R. C. Weins, R. Williams, J. Schieber, and J. Grotzinger (2015), Distribution of mineralized veins from Yellowknife Bay to Mount Sharp, Gale Crater, Mars: Insight from textural and compositional variations, Abstract 1903 presented at Lunar and Planet. Sci. Conf., 46.
- Kurepin, V. A. (2005), A thermodynamic model of Fe-Cr spinels, *Contrib. Mineral. Petrol.*, *149*, 591–599.
- Lanza, N., R. C. Wiens, W. W. Fischer, J. P. Grotzinger, A. Cousin, M. S. Rice, B. C. Clark, R. E. Arvidson, J. Hurowitz, and R. Gellert (2014), Observations of high manganese layers by the Curiosity rover at the Kimberley, Gale Crater, Mars, Abstract #P36A-06 presented AGU Fall Meeting Abstracts.
- Le Bas, M. J. (2008), Fenites associated with carbonatites, *Can. Mineral.*, *46*, 915–932, doi:10.3749/canmin.46.4.915.
- Le Deit, L., E. Hauber, F. Fueten, M. Pondrelli, A. P. Rossi, and R. Jaumann (2013), Sequence of infilling events in Gale Crater, Mars: Results from morphology, stratigraphy, and mineralogy, *J. Geophys. Res. Planets*, *118*, 2439–2473, doi:10.1002/2012JE004322.
- Le Deit, L., N. Mangold, O. Forni, D. Blaney, A. Cousin, G. Dromart, C. Fabre, M. Fisk, O. Gasnault, and N. Lanza (2015), The potassic sedimentary rocks in Gale crater, Mars as seen by ChemCam onboard Curiosity, Abstract #1438 presented at Lunar and Planet. Sci. Conf., 46.
- Le Maitre, R. W., A. Streckeisen, B. Zanettin, M. Le Bas, B. Bonin, and P. Bateman (2002), *Igneous Rocks: A Classification and Glossary of Terms: Recommendations of the International Union of Geological Sciences Subcommittee on the Systematics of Igneous Rocks*, Cambridge Univ. Press, New York.
- Legendre, C., R. Maury, M. Caroff, H. Guillou, J. Cotten, C. Chauvel, C. Bollinger, C. Hémond, G. Guille, and S. Blais (2005), Origin of exceptionally abundant phonolites on Ua Pou Island (Marquesas, French Polynesia): Partial melting of basanites followed by crustal contamination, *J. Petrol.*, *46*(9), 1925–1962.
- Levinstein, H. J., M. Robbins, and C. Capio (1972), A crystallographic study of the system  $\text{FeCr}_2\text{O}_4\text{-FeFe}_2\text{O}_4$  ( $\text{Fe}^{2+}\text{Fe}^{3+}_{(x)}\text{Cr}_{(2-x)}\text{O}_4$ ), *Mater. Res. Bull.*, *7*, 27–34.
- Lilova, K. I., F. Xu, K. M. Rosso, C. I. Pearce, S. Kamali, and A. Navrotsky (2012), Oxide melt solution calorimetry of  $\text{Fe}^{2+}$ -bearing oxides and application to the magnetite–maghemite ( $\text{Fe}_3\text{O}_4\text{-Fe}_8/3\text{O}_4$ ) system, *Am. Mineral.*, *97*, 164–175.
- Mahaffy, P. R., C. R. Webster, M. Cabane, P. G. Conrad, P. Coll, S. K. Atreya, R. Arvey, M. Barciniak, M. Benna, and L. Bleacher (2012), The sample analysis at Mars investigation and instrument suite, *Space Sci. Rev.*, *170*(1–4), 401–478.
- Marshall, B. D., H. H. Woodard, and D. J. DePaolo (1986), K-Ca-Ar systematics of authigenic sanidine from Waukau, Wisconsin, and the diffusivity of argon, *Geology*, *14*, 936–938.
- Martin, R. F. (1971), Disordered authigenic feldspars of the series  $\text{KAlSi}_3\text{O}_8\text{-KBSi}_3\text{O}_8$  from southern California, *Am. Mineral.*, *56*, 281–291.
- Martin, R. F. (2006), A-type granites of crustal origin ultimately result from open-system fenitization-type reactions in an extensional environment, *Lithos*, *91*(1), 125–136.
- McAdam, A. C., H. B. Franz, B. Sutter, P. D. Archer, C. Freissinet, J. L. Eigenbrode, D. W. Ming, S. K. Atreya, D. L. Bish, and D. F. Blake (2014), Sulfur-bearing phases detected by evolved gas analysis of the Rocknest aeolian deposit, Gale Crater, Mars, *J. Geophys. Res. Planets*, *119*, 373–393, doi:10.1002/2013JE004518.
- McAdam, A. C., P. D. Archer, B. Sutter, H. B. Franz, J. L. Eigenbrode, D. W. Ming, R. V. Morris, P. B. Niles, J. C. Stern, and C. Freissinet (2015), Major volatiles from MSL SAM evolved gas analyses: Yellowknife Bay through lower mount sharp, paper presented at Lunar and Planet. Sci. Conf.
- McLennan, S. M., et al. (2014), Elemental geochemistry of sedimentary rocks at Yellowknife Bay, Gale Crater, Mars, *Science*, *343*(6169), doi:10.1126/science.1244734.
- McSween, H. Y., and A. H. Treiman (1998), Martian samples, in *Planetary Materials, Reviews in Mineralogy*, vol. 36, edited by J. J. Papike, pp. 6–1–6–53, Mineral. Soc. of Am., Washington, D. C.
- McSween, H. Y., M. B. Wyatt, R. Gellert, J. Bell, R. V. Morris, K. E. Herkenhoff, L. S. Crumpler, K. A. Milam, K. R. Stockstill, and L. L. Tornabene (2006), Characterization and petrologic interpretation of olivine-rich basalts at Gusev Crater, Mars, *J. Geophys. Res.*, *111*, E02S10, doi:10.1029/2005JE002477.
- McSween, H. Y., T. C. Labotka, and C. E. Viviano-Beck (2015), Metamorphism in the Martian crust, *Meteorit. Planet. Sci.*, *50*(4), 590–603.
- Ming, D. W., R. Gellert, R. V. Morris, R. E. Arvidson, J. Brueckner, B. C. Clark, B. A. Cohen, C. d'Uston, T. Economou, and I. Fleischer (2008), Geochemical properties of rocks and soils in Gusev Crater, Mars: Results of the alpha particle X-ray spectrometer from Cumberland Ridge to Home Plate, *J. Geophys. Res.*, *113*, E12S39, doi:10.1029/2008JE003195.
- Montanari, A. (1991), Authigenesis of impact spheroids in the K/T boundary clay from Italy: New constraints for high-resolution stratigraphy of terminal Cretaceous events, *J. Sediment. Petrol.*, *61*, 315–339.
- Morogan, V., and R. F. Martin (1985), Mineralogy and partial melting of fenitized crustal xenoliths in the Oldoinyo Lengai carbonatitic volcano, Tanzania, *Am. Mineral.*, *70*, 1114–1126.
- Morris, R. V., G. Klingelhoefer, B. Bernhardt, C. Schröder, D. S. Rodionov, P. De Souza, A. Yen, R. Gellert, E. Evlanov, and J. Foh (2004), Mineralogy at Gusev Crater from the Mössbauer spectrometer on the Spirit Rover, *Science*, *305*(5685), 833–836.
- Morris, R. V., et al. (2013), The amorphous component in Martian basaltic soil in global perspective from MSL and MER missions, Abstract 1653 presented at Lunar and Planet. Sci. Conf.
- Morrison, S. M., et al. (2015), Crystal-chemical analysis of Martian minerals in Gale Crater, Abstract 2056 presented at Lunar and Planet. Sci. Conf. 46.
- Muttik, N., F. M. McCubbin, L. P. Keller, A. R. Santos, W. A. McCutcheon, P. P. Provencio, Z. Rahman, C. K. Shearer, J. W. Boyce, and C. B. Agee (2014), Inventory of  $\text{H}_2\text{O}$  in the ancient Martian regolith from Northwest Africa 7034: The important role of Fe oxides, *Geophys. Res. Lett.*, *41*, 8235–8244, doi:10.1002/2014GL02533.
- Nachon, M., S. Clegg, N. Mangold, S. Schröder, L. Kah, G. Dromart, A. Ollila, J. Johnson, D. Oehler, and J. Bridges (2014), Calcium sulfate veins characterized by ChemCam/Curiosity at Gale Crater, Mars, *J. Geophys. Res. Planets*, *119*, 1991–2016, doi:10.1002/2013JE004588.

- Nekvasil, H., A. Dondolini, J. Horn, J. Filiberto, H. Long, and D. H. Lindsley (2004), The origin and evolution of silica-saturated alkalic suites: An experimental study, *J. Petrol.*, *45*(4), 693–721.
- Nekvasil, H., J. Filiberto, F. M. McCubbin, and D. H. Lindsley (2007), Alkalic parental magmas for chassignites?, *Meteorit. Planet. Sci.*, *42*(6), 979–992.
- Nisbet, E. G. (1987), *Young Earth: An Introduction to Archean Geology*, Springer Science and Business Media, Netherlands.
- O'Neil, J., C. Maurice, R. K. Stevenson, J. Larocque, C. Cloquet, J. David, and D. Francis (2007), The geology of the 3.8 Ga Nuvvuagittuq (Porpoise Cove) greenstone belt, northeastern Superior province, Canada, *Dev. Precambrian Geol.*, *15*, 219–250.
- O'Neil, J., R. W. Carlson, D. Francis, and R. K. Stevenson (2008), Neodymium-142 evidence for Hadean mafic crust, *Science*, *321*(5897), 1828–1831.
- O'Neil, J., R. W. Carlson, J.-L. Paquette, and D. Francis (2012), Formation age and metamorphic history of the Nuvvuagittuq Greenstone Belt, *Precambrian Res.*, *220*, 23–44.
- O'Hanley, D. S. (1996), *Serpentinites: Records of Tectonic and Petrological History*, 277 pp., Oxford Univ. Press, New York.
- Okeruda, H. (1997), Single-crystal X-ray studies of cation-deficient magnetite, *Z. Kristallogr.*, *212*, 458–461.
- O'Neil, H. S. C., H. Annersten, and D. Virgo (1992), The temperature dependence of the cation distribution in magnesioferrite (MgFe<sub>2</sub>O<sub>4</sub>) from powder XRD structural refinements and Mössbauer spectroscopy, *Am. Mineral.*, *77*, 725–740.
- Özdemir, Y., J. Blundy, and N. Güleç (2011), The importance of fractional crystallization and magma mixing in controlling chemical differentiation at Süphan stratovolcano, eastern Anatolia, Turkey, *Contrib. Mineral. Petrol.*, *162*(3), 573–597.
- Palucis, M. C., W. E. Dietrich, A. G. Hayes, R. M. Williams, S. Gupta, N. Mangold, H. Newsom, C. Hardgrove, F. Calef, and D. Y. Sumner (2014), The origin and evolution of the Peace Vallis fan system that drains to the Curiosity landing area, Gale Crater, Mars, *J. Geophys. Res. Planets*, *119*, 705–728, doi:10.1002/2013JE004583.
- Papike, J. J., J. Karner, C. Shearer, and P. Burger (2009), Silicate mineralogy of Martian meteorites, *Geochim. Cosmochim. Acta*, *73*(24), 7443–7485.
- Parfitt, R., S. Van der Gaast, and C. Childs (1992), A structural model for natural siliceous ferrihydrite, *Clays Clay Miner.*, *40*, 675–675.
- Pesonen, L., C. Koeberl, and H. Hautaniemi (2003), Airborne geophysical survey of the Lake Bosumtwi meteorite impact structure (southern Ghana)—Geophysical maps with descriptions, *Jahrb. Geol. Bundesanst., Vienna* (Yearbook of the Austrian Geological Survey), *143*, 581–604.
- Pilet, S., M. B. Baker, and E. M. Stolper (2008), Metasomatized lithosphere and the origin of alkaline lavas, *Science*, *320*(5878), 916–919.
- Pirajno, F. (2005), Hydrothermal processes associated with meteorite impact structures: Evidence from three Australian examples and implications for economic resources, *Aust. J. Earth Sci.*, *52*, 587–605.
- Pirajno, F. (2009), Hydrothermal processes associated with meteorite impacts, in *Hydrothermal Processes and Mineral Systems*, edited by F. Pirajno, pp. 1097–1130, Springer, Netherlands, doi:10.1007/978-1-4020-8613-7\_11.
- Pirajno, F. (2013), Effects of metasomatism on mineral systems and their host rocks: Alkali metasomatism, skarns, greisens, tourmalinites, rodingites, black-wall alteration and listvenites, in *Metasomatism and the Chemical Transformation of Rock*, edited by D. Harlov and H. Austrheim, pp. 203–251, Springer, New York.
- Rampe, E., M. Kraft, T. Sharp, D. Golden, D. Ming, and P. Christensen (2012), Allophane detection on Mars with thermal emission spectrometer data and implications for regional-scale chemical weathering processes, *Geology*, *40*(11), 995–998.
- Ribbe, P. H. (1975), Optical properties and lattice parameters of plagioclase feldspars, in *Feldspar Mineralogy*, *Mineralogical Society of America Short Course Notes*, edited by P. H. Ribbe, pp. R53–R72, Southern Printing Company, Blacksburg, Va.
- Santos, A. R., C. B. Agee, F. M. McCubbin, C. K. Shearer, P. V. Burger, R. Tartèse, and M. Anand (2015), Petrology of igneous clasts in Northwest Africa 7034: Implications for the petrologic diversity of the Martian crust, *Geochim. Cosmochim. Acta*, *157*, 56–85.
- Sautter, V., C. Fabre, O. Forni, M. Toplis, A. Cousin, A. Ollila, P. Meslin, S. Maurice, R. Wiens, and D. Baratoux (2014), Igneous mineralogy at Bradbury Rise: The first ChemCam campaign at Gale crater, *J. Geophys. Res. Planets*, *119*, 30–46, doi:10.1002/2013JE004472.
- Sautter, V., M. Toplis, R. Wiens, A. Cousin, C. Fabre, O. Gasnault, S. Maurice, O. Forni, J. Lasue, and A. Ollila (2015), In situ evidence for continental crust on early Mars, *Nat. Geosci.*, doi:10.1038/NGEO2474.
- Schmidbauer, E., and M. Keller (2006), Magnetic hysteresis properties, Mössbauer spectra and structural data of spherical 250 nm particles of solid solutions Fe<sub>3</sub>O<sub>4</sub> – γ-Fe<sub>2</sub>O<sub>3</sub>, *J. Magn. Magn. Mater.*, *297*, 107–117.
- Schmidt, M., M. Baker, J. Berger, M. Fisk, R. Gellert, S. McLennan, M. Newcombe, E. Stolper, and L. Thompson (2014a), Diverse, alkali-rich igneous and volcanoclastic rocks reflect a metasomatized mantle beneath Gale crater, Abstract P33E-06 presented at American Geophysical Union Fall Meeting.
- Schmidt, M., J. Campbell, R. Gellert, G. Perrett, A. Treiman, D. Blaney, A. Ollila, F. Calef, L. Edgar, and B. Elliott (2014b), Geochemical diversity in first rocks examined by the Curiosity Rover in Gale Crater: Evidence for and significance of an alkali and volatile-rich igneous source, *J. Geophys. Res. Planets*, *119*, 64–81, doi:10.1002/2013JE004481.
- Schwenzer, S. P., and D. A. Kring (2013), Alteration minerals in impact-generated hydrothermal systems—Exploring host rock variability, *Icarus*, *226*(1), 487–496.
- Schwenzer, S. P., O. Abramov, C. Allen, J. Bridges, S. Clifford, J. Filiberto, D. Kring, J. Lasue, P. McGovern, and H. Newsom (2012), Gale Crater: Formation and post-impact hydrous environments, *Planet. Space Sci.*, *70*(1), 84–95.
- Schwertmann, U., and E. Murad (1990), The influence of aluminum on iron oxides: XIV. Al-substituted magnetite synthesized at ambient temperatures, *Clays Clay Miner.*, *38*, 196–202.
- Schwertmann, U., J. Friedl, and H. Stanjek (1999), From Fe(III) ions to ferrihydrite and then to hematite, *J. Colloid Interface Sci.*, *209*(1), 215–223.
- Shearer, C. K., P. V. Burger, J. J. Papike, L. E. Borg, A. J. Irving, and C. D. K. Herd (2008), Petrogenetic linkages among Martian basalts: Implications based on trace element chemistry of olivine, *Meteorit. Planet. Sci.*, *43*, 1241–1258.
- Shi, G., P. Tropper, and R. Zhu (2009), The occurrence of magnesioferrite-rich spinels in a trachyandesite from NE China, *Mineral. Petrol.*, *95*, 125–134.
- Siebach, K., J. Grotzinger, S. McLennan, J. Hurowitz, D. Ming, D. Vaniman, E. Rampe, D. Blaney, and L. Kah (2015), Constraining the texture and composition of pore-filling cements at Gale crater, Mars, Abstract 2234 presented at Lunar and Planet. Sci. Conf.
- Sillitoe, R. H. (2010), Porphyry copper systems, *Econ. Geol.*, *105*, 3–41.
- Smithies, R. H., and D. C. Champion (1999), Late Archaean felsic alkaline igneous rocks in the Eastern Goldfields, Yilgarn Craton, Western Australia: A result of lower crustal delamination?, *J. Geol. Soc.*, *156*(3), 561–576.
- Squyres, S. W., and A. H. Knoll (2005), Sedimentary rocks at Meridiani Planum: Origin, diagenesis, and implications for life on Mars, *Earth Planet. Sci. Lett.*, *240*(1), 1–10.
- Stack, K., J. Grotzinger, S. Gupta, L. Kah, K. Lewis, M. McBride, M. Minitti, D. Rubin, J. Schieber, and D. Sumner (2015), Sedimentology and stratigraphy of the Pahrump Hills outcrop, lower Mount Sharp, Gale Crater, Mars, Abstract #1994 presented at Lunar and Planet. Sci. Conf.
- Stern, J. C., et al. (2015a), Evidence for indigenous nitrogen in sedimentary and aeolian deposits from the Curiosity rover investigations at Gale Crater, Mars, *Proc. Natl. Acad. Sci. U.S.A.*, *112*(14), 4245–4250, doi:10.1073/pnas.1420932112.

- Stern, J. C., et al. (2015b), The nitrate/perchlorate ratio on Mars as an indicator for habitability, Abstract 2590 presented at Lunar and Planet. Sci. Conf.
- Stolper, E. M., M. B. Baker, M. E. Newcombe, M. E. Schmidt, A. Treiman, A. Cousin, M. D. Dyar, M. R. Fisk, R. Gellert, and P. L. King (2013), The petrochemistry of Jake\_M: A Martian mugearite, *Science*, *341*(6153), doi:10.1126/science.1239463.
- Sutcliffe, R. H., A. R. Smith, W. Doherty, and R. L. Barnett (1990), Mantle derivation of Archean amphibole-bearing granitoid and associated mafic rocks: Evidence from the southern Superior Province, Canada, *Contrib. Mineral. Petrol.*, *105*(3), 255–274.
- Sutter, B., E. Heil, R. Morris, P. Archer, D. Ming, P. Niles, J. Eignebrode, H. Franz, C. Freissinet, and D. Glavin (2015), The investigation of perchlorate/iron phase mixtures as a possible source of oxygen detected by the Sample Analysis at Mars (SAM) instrument in Gale Crater, Mars, Abstract 2137 presented at Lunar and Planet. Sci. Conf.
- Takagi, J., M. Ozaki, S. Kazuhiro, and T. Mizoguchi (2010), Chlorine occupancy dependence of crystal structure of pure  $\beta$ -phase of iron-oxyhydroxide, *Mater. Trans.*, *51*(7), 1330–1339.
- Taroev, V., J. Göttlicher, H. Kroll, A. Kashaev, L. Suvorova, H. Pentinghaus, H. Bernotat-Wulf, U. Breit, V. Tauson, and V. Laskevich (2008), Synthesis and structural state of K-feldspars in the system  $K[AlSi_3O_8]-K[FeSi_3O_8]$ , *Eur. J. Mineral.*, *20*, 635–651.
- Taylor, G. J. (2013), The bulk composition of Mars, *Chem. Erde-Geochem.*, *73*(4), 401–420.
- Taylor, S. R., and S. McLennan (2009), *Planetary Crusts: Their Composition, Origin and Evolution*, Cambridge Univ. Press, Cambridge, U. K.
- Thomas, W. A. (2011), Detrital-zircon geochronology and sedimentary provenance, *Lithosphere*, *3*(4), 304–308.
- Thompson, L. M., M. E. Schmidt, G. Perrett, B. Elliott, R. Gellert, and M. Fisk (2014), K-rich rocks at Gale, Dingo Gap to the Kimberley: An APXS perspective, Abstract 1433 presented at Eighth International Conference on Mars.
- Thomson, B. J., N. T. Bridges, R. Milliken, A. Baldrige, S. J. Hook, J. K. Crowley, G. M. Marion, C. R. de Souza Filho, A. J. Brown, and C. M. Weitz (2011), Constraints on the origin and evolution of the layered mound in Gale Crater, Mars using Mars Reconnaissance Orbiter data, *Icarus*, *214*(2), 413–432.
- Treiman, A. H., and J. Filiberto (2015), Geochemical diversity of shergottite basalts: Mixing and fractionation, and their relation to Mars surface basalts, *Meteorit. Planet. Sci.*, *50*(4), 632–648.
- Treiman, A. H., M. J. Drake, M.-J. Janssens, R. Wolf, and M. Ebihara (1986), Core formation in the Earth and shergottite parent body (SPB): Chemical evidence from basalts, *Geochim. Cosmochim. Acta*, *50*(6), 1071–1091.
- Treiman, A. H., et al. (2014), Ferrian saponite from the Santa Monica Mountains (California, U.S.A., Earth): Characterization as an analog for clay minerals on Mars with application to Yellowknife Bay in Gale Crater, *Am. Mineral.*, *99*, 2234–2250.
- Valley, J. W., W. H. Peck, E. M. King, and S. A. Wilde (2002), A cool early Earth, *Geology*, *30*(4), 351–354.
- Vaniman, D. T., et al. (2014), Mineralogy of a mudstone at Yellowknife Bay, Gale Crater, Mars, *Science*, *343*(6169), doi:10.1126/science.1243480.
- Vasconcelos, M. A. R., E. P. Leite, and A. P. Crosta (2012), Contributions of gamma-ray spectrometry to terrestrial impact crater studies: The example of Serra da Cangalha, northeastern Brazil, *Geophys. Res. Lett.*, *39*, L04306, doi:10.1029/2011GL050525.
- Walker, T. R., B. Waugh, and A. J. Grone (1978), Diagenesis in first-cycle desert alluvium of Cenozoic age, southwestern United States and northwestern Mexico, *Geol. Soc. Am. Bull.*, *89*, 19–32.
- Wechsler, B. A., D. H. Lindsley, and C. T. Prewitt (1984), Crystal structure and cation distribution in titanomagnetites ( $Fe_{3-x}Ti_xO_4$ ), *Am. Mineral.*, *69*, 754–770.
- Whitaker, M. L., H. Nekvasil, D. H. Lindsley, and N. J. DiFrancesco (2007), The role of pressure in producing compositional diversity in intraplate basaltic magmas, *J. Petrol.*, *48*(2), 365–393.
- Whitaker, M. L., H. Nekvasil, D. H. Lindsley, and M. McCurry (2008), Can crystallization of olivine tholeiite give rise to potassic rhyolites?—An experimental investigation, *Bull. Volcanol.*, *70*(3), 417–434.
- Wiens, R. C., and S. Maurice (2015), ChemCam: Chemostratigraphy by the First Mars Microprobe, *Elements*, *11*(1), 33–38.
- Wiens, R. C., S. Maurice, B. Barraclough, M. Saccoccio, W. C. Barkley, J. F. Bell III, S. Bender, J. Bernardin, D. Blaney, and J. Blank (2012), The ChemCam instrument suite on the Mars Science Laboratory (MSL) rover: Body unit and combined system tests, *Space Sci. Rev.*, *170*(1–4), 167–227.
- Williams, H., F. J. Turner, and C. M. Gilbert (1982), *Petrography: An Introduction to the Study of Rocks in Thin Section*, 2nd ed., W. H. Freeman, New York.
- Wilson, M. (1989), *Igneous Petrogenesis: A Global Tectonic Approach*: London, Unwyn Hyman, London.
- Winter, J. D. (2010), *Principles of Igneous and Metamorphic Petrology*, 2nd ed., Prentice Hall, New York.
- Wittmann, A., R. L. Korotev, B. L. Jolliff, A. J. Irving, D. E. Moser, I. Barker, and D. Rumble III (2015), Petrography and composition of Martian regolith breccia meteorite Northwest Africa 7475, *Meteorit. Planet. Sci.*, *50*, 326–352.
- Woodard, H. H. (1972), Syngenetic sanidine beds from Middle Ordovician Saint Peter Sandstone, Wisconsin, *J. Geol.*, *80*, 323–332.
- Wray, J. J., S. T. Hansen, J. Dufek, G. A. Swayze, S. L. Murchie, F. P. Seelos, J. R. Skok, R. P. Irwin III, and M. S. Ghiorso (2013), Prolonged magmatic activity on Mars inferred from the detection of felsic rocks, *Nat. Geosci.*, *6*(12), 1013–1017.
- Wright, T. L., and D. B. Stewart (1968), X-ray and optical study of alkali feldspar: I. Determination of composition and structural state from refined unit-cell parameters and 2V, *Am. Mineral.*, *53*, 38–87.
- Wyllie, P. J. (1977), Mantle fluid compositions buffered by carbonates in peridotite- $CO_2$ - $H_2O$ , *J. Geol.*, *85*, 187–207.
- Yen, A. S., R. Gellert, C. Schröder, R. V. Morris, J. F. Bell, A. T. Knudson, B. C. Clark, D. W. Ming, J. A. Crisp, and R. E. Arvidson (2005), An integrated view of the chemistry and mineralogy of Martian soils, *Nature*, *436*(7047), 49–54.
- Zozulya, D. R., T. B. Bayanova, and G. N. Eby (2005), Geology and age of the late Archean Keivy alkaline province, Northeastern Baltic Shield, *J. Geol.*, *113*(5), 601–608.